



3 4456 0055254 1

ORNL/TM-9710

oml

OAK RIDGE
NATIONAL
LABORATORY

MARTIN MARIETTA

TSX Graphite for Extended Use in the N-Reactor

C. R. Kennedy

OAK RIDGE NATIONAL LABORATORY
CENTRAL RESEARCH LIBRARY
CIRCULATION SECTION
EVEN ROOM 117

LIBRARY LOAN COPY

DO NOT TRANSFER TO ANOTHER PERSON

If you wish someone else to see this
report, send in name with report and
the library will arrange a loan.

OPERATED BY
MARTIN MARIETTA ENERGY SYSTEMS, INC.
FOR THE UNITED STATES
DEPARTMENT OF ENERGY



Printed in the United States of America. Available from
National Technical Information Service
U.S. Department of Commerce
5285 Port Royal Road, Springfield, Virginia 22161
NTIS price codes—Printed Copy: A04; Microfiche A01

This report was prepared as an account of work sponsored by an agency of the United States Government. Neither the United States Government nor any agency thereof, nor any of their employees, makes any warranty, express or implied, or assumes any legal liability or responsibility for the accuracy, completeness, or usefulness of any information, apparatus, product, or process disclosed, or represents that its use would not infringe privately owned rights. Reference herein to any specific commercial product, process, or service by trade name, trademark, manufacturer, or otherwise, does not necessarily constitute or imply its endorsement, recommendation, or favoring by the United States Government or any agency thereof. The views and opinions of authors expressed herein do not necessarily state or reflect those of the United States Government or any agency thereof.

METALS AND CERAMICS DIVISION

TSX GRAPHITE FOR EXTENDED USE IN THE N-REACTOR

C. R. Kennedy

Date Published -- August 1985

Prepared for
United Nuclear, Inc.
Richland, Washington

Prepared by the
OAK RIDGE NATIONAL LABORATORY
Oak Ridge, Tennessee 37831
operated by
MARTIN MARIETTA ENERGY SYSTEMS, INC.
for the
U.S. DEPARTMENT OF ENERGY
under Contract No. DE-AC05-84OR21400



3 4456 0055254 1

CONTENTS

ABSTRACT 1

INTRODUCTION 1

IRRADIATION DAMAGE 3

DIMENSIONAL CHANGES 4

FRACTURE STRENGTH 16

MODULUS OF ELASTICITY 25

THERMAL CONDUCTIVITY 25

COEFFICIENTS OF THERMAL EXPANSION 27

IRRADIATION CREEP 27

USEFUL LIFE AND APPROXIMATE STRESS CALCULATIONS 39

SUMMARY 47

ACKNOWLEDGMENTS 48

REFERENCES 48

Appendix A. THERMAL CONDUCTIVITY DATA 51

Appendix B. CONFIRMATION OF EQUATION 15 59

TSX GRAPHITE FOR EXTENDED USE IN THE N-REACTOR

C. R. Kennedy

ABSTRACT

The N-Reactor at Hanford has been in operation since the mid-1960s. In view of the large cost required for replacement of this reactor, it was desirable to consider the merits and risks of prolonged extension of the operational life of the present reactor. Continued operation would require careful attention to the effects of dimensional changes of the core graphite under irradiation. Not only are the free-dimensional changes of importance, but also the effects of restrained growth on physical properties and strength.

This report reviews the limited amount of irradiation data available for grade TSX graphite with the purpose of obtaining reasonable estimates of material behavior. The results are enhanced by obtaining generalized behavior characteristics demonstrated by similar grades of graphite, such as CSF, AGOT, and PGA. The intent of this work is to furnish the necessary coefficients to describe the material behavior for inclusion in the constitutive equations for the anisotropic graphite grade TSX.

Estimates of the free-dimensional changes of TSX graphite as a function of temperature and fluence have been made and shown to be in good agreement with the data. The effects of irradiation on other physical properties, such as elastic moduli, conductivity, and coefficient of thermal expansion, are also described. The irradiation creep characteristics of TSX graphite are also estimated on the basis of data for similar grades of graphite in the United States and Europe. Crude approximations of stresses generated in the keyed structure were made to demonstrate the magnitude of the problem. The results clearly predict that the filler-block keys will fail and the tube-block keys will not. It is also indicated that the overall stack height growth will be increased by 25 to 38 mm (1-1.5 in.) because of creep. A more detailed analysis should be done to confirm these approximations.

INTRODUCTION

The first controlled nuclear-fission reactor at the University of Chicago used graphite as the moderator and reflector. This graphite was

similar to premium electrode grades, the only graphites available at the time in the appropriate purity and sizes. Made of highly anisotropic filler particles and a coal-tar pitch binder, it was extruded, baked, and impregnated before graphitization. This graphite was the nuclear standard in the early reactors. The prototype production reactor at Oak Ridge, all of the Hanford production reactors, and the initial gas-cooled power reactors in the United States, France, and England through the 1950s and into the 1960s used graphites of this type. These graphites performed very well in such reactor systems with low temperatures, fairly low power densities, and fairly low total flux accumulation. However, as operating temperatures and power densities were increased to obtain greater efficiency, the demands of the operating systems began to exceed the capabilities of the first-generation graphites, so a series of newer second-generation graphites was developed to meet the more demanding requirements.

The N-Reactor at Hanford is a transition reactor linking the initial production reactor to the newer high-temperature systems useful for steam production and electric generating capabilities. The TSX graphite used, however, is a first-generation material with highly anisotropic properties. The initial design requirements were well within the capabilities of TSX, but the high cost required for replacing this reactor makes it desirable to consider the possibility of extending the use of the N-Reactor rather than replacing it.

Continued operation of the core requires that careful attention be given to the dimensional changes produced in the graphite by irradiation. The neutron flux and temperature gradients in the graphite moderator blocks result in a time-varying differential growth. The resulting stresses in many cases are similar to thermal stresses produced by an ever-increasing temperature gradient. Graphite, fortunately, has the ability to creep under irradiation, allowing the stress intensity generated by the differential growth to relax and, with proper design, to remain below critical levels for fracture. The creep also averages the free-dimensional changes, contributing to the dimensional stability of the core structure. In the N-Reactor, however, there is the additional problem of stress concentrations due to the keyed structure.

It is not within the scope of this report to furnish in-depth stress-intensity calculations assessing the behavior of graphite throughout the life of the N-Reactor. It is, however, the intent to furnish the necessary coefficients describing the material behavior for inclusion in the constitutive equations, which have the following form:

$$\begin{aligned} (\text{total strain}) = & (\text{elastic strain}) + (\text{creep strain}) \\ & + (\text{irradiation growth}) + (\text{thermal growth}) \end{aligned} .$$

In this context, a review of the results of past irradiation experiments is beneficial in order to obtain reliable estimates of the material behavior. The irradiation data are very limited for TSX graphite, and the overall results rely heavily on data obtained on similar grades such as CSF, AGOT, and PGA. There is also a significant amount of information from irradiation of second-generation grades to, or perhaps past, useful life exposures but at temperatures above the N-Reactor operating temperatures. These results furnish generalized behavior characteristics that can be extended to the more anisotropic graphites such as grade TSX.

IRRADIATION DAMAGE

The effect of irradiation on the graphite crystal is displacement damage caused by collision of energetic neutrons with the carbon atoms in the lattice. The carbon atoms in the hexagonal layer planes are displaced to form interstitials between the layer planes, leaving vacancies in the original planes. The consequence of the displacement is largely a function of the irradiation temperature and the mobility of the interstitials. At fairly low temperatures (below room temperature) the interstitials are essentially immobile and form point defects. As the temperature increases, the interstitials form dipoles and then planes as interstitials cluster. The exact mechanisms of the formation of new hexagonal planes and collapse of the layer planes in the α -axis direction are still not complete and will not be discussed in detail. Several reviews furnish fairly complete bibliographies on this subject. Notable are those by deHalas,¹ Reynolds,² Simmons,³ Kelly,⁴ Thrower,⁵ and Engle and Eatherly.⁶

The major transition temperature determined in annealing studies that is significant to the N-Reactor irradiation is around 300 to 350°C, where interstitial clusters become mobile. Below this temperature range the lattice is severely distorted by irradiation damage, and energy storage must be a real consideration. Above 400°C, because of interstitial mobility, the lattice is only slightly distorted until the normal ABAB hexagonal stacking is altered to a randomized ABC stacking. This occurs as the interstitial planes grow to become very large and the lattice spacing returns to the initial graphite spacing. Bokros⁷ has shown that there appears to be an increase in growth rate with increasing temperature; however, the growth rate increase was also shown to depend on the crystallite size in the polycrystalline aggregate. The more perfect crystalline graphite with a large crystallite size has lower growth rates at higher temperature than the less graphitic materials. This effect is related to the increased probability of vacancy-interstitial recombination and annihilation in the materials with larger crystallite size. However, this effect is not very large until the irradiation temperature exceeds 500 to 600°C.

DIMENSIONAL CHANGES

The dimensional changes of the highly anisotropic, hexagonal crystal structure caused by neutron irradiation are fairly large. The *c*-axis growth and the *a*-axis shrinkage in single crystals or in highly aligned pyrographites have been shown to produce up to 800% dimensional changes without volume changes or structural degradation other than shape change. However, reactor-grade graphites are polycrystalline, and even the more anisotropic grades are still aggregates of crystals with varying mismatch angles between the individual crystals and crystallites. The polycrystalline graphite structures also include porosity consisting of both inter- and intraparticle porosity associated with either crystallite boundaries or particle boundaries. Thus, the averaging techniques required to translate the single-crystal dimensional changes to polycrystalline graphites must include the additional effects of porosity

changes and shearing stresses. The various methods of averaging are given in the previously mentioned reviews.¹⁻⁶ Each method has been essentially a modification of the averaging technique used by Bacon⁸ for the coefficient of thermal expansion. The following is an extension of the treatment used by Price and Bokros⁹ in explaining the dimensional changes in polycrystalline graphite. The expression

$$\frac{\lambda}{\lambda_x} \frac{d\lambda_x}{d\gamma} = (1 - R_x) G_{x,c} \frac{\lambda}{\lambda_c} \frac{d\lambda_c}{d\gamma} + R_x G_{x,a} \frac{\lambda}{\lambda_a} \frac{d\lambda_a}{d\gamma}, \quad (1)$$

where γ is the neutron fluence and R_x is determined from X-ray diffraction data and depends on the intensity of the preferred orientation. $G_{x,c}$ and $G_{x,a}$ are accommodation factors, which are the fractions of a -axis and c -axis growth that are realized in the overall growth of the graphite. Initially, $G_{x,c}$ is fairly small because of the large quantity of microcracks parallel to the basal planes. However, as the c -axis irradiation growth fills these pores, $G_{x,c}$ increases to a value approaching unity. On the other hand, $G_{x,a}$ is essentially equal to unity because void formation and microcracking normal to the basal planes are very rare. In fact, in the low fluence results and comparisons, $G_{x,a}$ has been essentially equal to unity and has been ignored. However, as G_{xmc} increases to unity and the growth accommodation by the preexisting microcracks is exhausted, the differential growth between the higher angle boundaries exceeds the fracture strength and new porosity is created. This porosity is normal to the basal planes, and $G_{x,a}$ begins to decrease in value.

The volume decrease (or bulk density increase) occurs when the value of $G_{x,c}$ is small; when the accommodating microcracks are exhausted and $G_{x,c}$ reaches unity, the densification is completed. The volume expands or the bulk density decreases as $G_{x,a}$ decreases in value. It is clear that both $G_{x,c}$ and $G_{x,a}$ are averages due to the preferred orientation distributions in various graphites and do not simply change in value independently. Considerable evidence¹⁰⁻¹² from surface area measurements and fracture toughness studies indicates that the large pores are reduced in size. But, there is a large increase in the number of small pores

beginning with the initial exposure to irradiation. Of course, the reduction in size of the large pores is limited, and the eventual saturation occurs as maximum density is obtained. The volume increase then occurs by an increase in the number of small pores in the graphite. The pore morphology and how it changes are important in understanding the overall dimensional changes in graphites and the ability to estimate those changes. It is also extremely important in an understanding of the fracture characteristics of irradiated graphite.

Estimates of the accommodation factor, $G_{x,c}$, have been made from the coefficients of thermal expansions.^{2,3,9} However, these estimates are valid only for the initial growth rates because $G_{x,c}$ is only reasonably constant in the preferred c -axis direction and begins to increase almost immediately in this direction in extruded anisotropic graphites. However, the magnitude of the volume change at a given irradiation temperature can be estimated by a consideration of both the overall porosity created by fabrication and that of the microcracking caused by cooling polycrystalline graphite from graphitization temperatures.¹³ Also, as the irradiation temperature is increased, the accommodation in the c -axis by microcracking is reduced significantly.¹³ This results in a reduction in the overall volume decrease and the fluence required to obtain the maximum densification. Therefore, the fluence necessary to seriously degrade the physical properties is reduced as irradiation temperature increases.

Only one irradiation experiment has been performed on TSX graphite to large fluences at or near the N-Reactor temperature. However, several graphites very similar to TSX have been irradiated over a fairly wide range of temperatures. These irradiations were performed by Helm¹⁴ and Henson et al.¹⁵ on CSF, AGOT, TSX, and PGA graphites. All of these materials were made by extrusion with similar filler cokes, binders, and impregnants, yielding very similar structures and anisotropy. Grade TSX does have a somewhat finer particle size, slightly higher density, and a slightly greater degree of anisotropy. These differences are minor and should only slightly affect the irradiation characteristics of TSX as compared with the other grades. One problem in these experiments is that the irradiation temperatures varied as much as 100°C in the General Electric Test Reactor (GETR) experiments during the irradiation cycle. The

reported temperatures are time-weighted average temperatures with some level of uncertainty. It is probably safe to say that the variability in the irradiation experiments is sure to exceed some of the minor differences due to grade.

Because we are more interested in the long-term irradiation behavior of the graphites, there are several specific characteristics that can be compared. The characteristics of density change are the maximum densification, the fluence to obtain maximum densification, and the fluence to achieve a density equal to the initial density. The dimensional change characteristics include the maximum shrinkage, the fluence to return to the initial length, and the fluence to grow 5% in the transverse direction. The maximum densification of the various grades as a function of irradiation temperature is shown in Fig. 1. The reduced densification with increasing temperature is in agreement with Kennedy¹¹ as described above. The fluence required to obtain the maximum densification is compared in Fig. 2 with the fluence required to achieve the initial density. This figure also illustrates the reduced life expectancy with increased irradiation temperature. Shown in Fig. 3 is the magnitude of the negative transverse strain as a function of irradiation temperature. These results are consistent with the small differences observed between the grades in Fig. 1. The fluences for the transverse strain to return to zero and to grow 5% are given in Fig. 4. Note that the data do not produce smooth curves in all cases, which is not unexpected in view of the experimental uncertainties. However, the good agreement between grades and the total overall consistency support the usefulness of the data for estimating TSX dimensional changes. The main area of uncertainty, unfortunately, is in the CSF data below 500°C (not shown in Figs. 2-4) that is in conflict with PGA results and inconsistent with higher-temperature CSF and AGOT results. These low-temperature CSF results are excluded even though there is presently no apparent justification other than the apparent lack of agreement with other data.

By using the results of Figs. 3 and 4 describing the transverse displacements, several significant points describing the growth can be located: the point of maximum contraction, the fluence required to expand back to zero, and the fluence required for 5% growth. By locating these

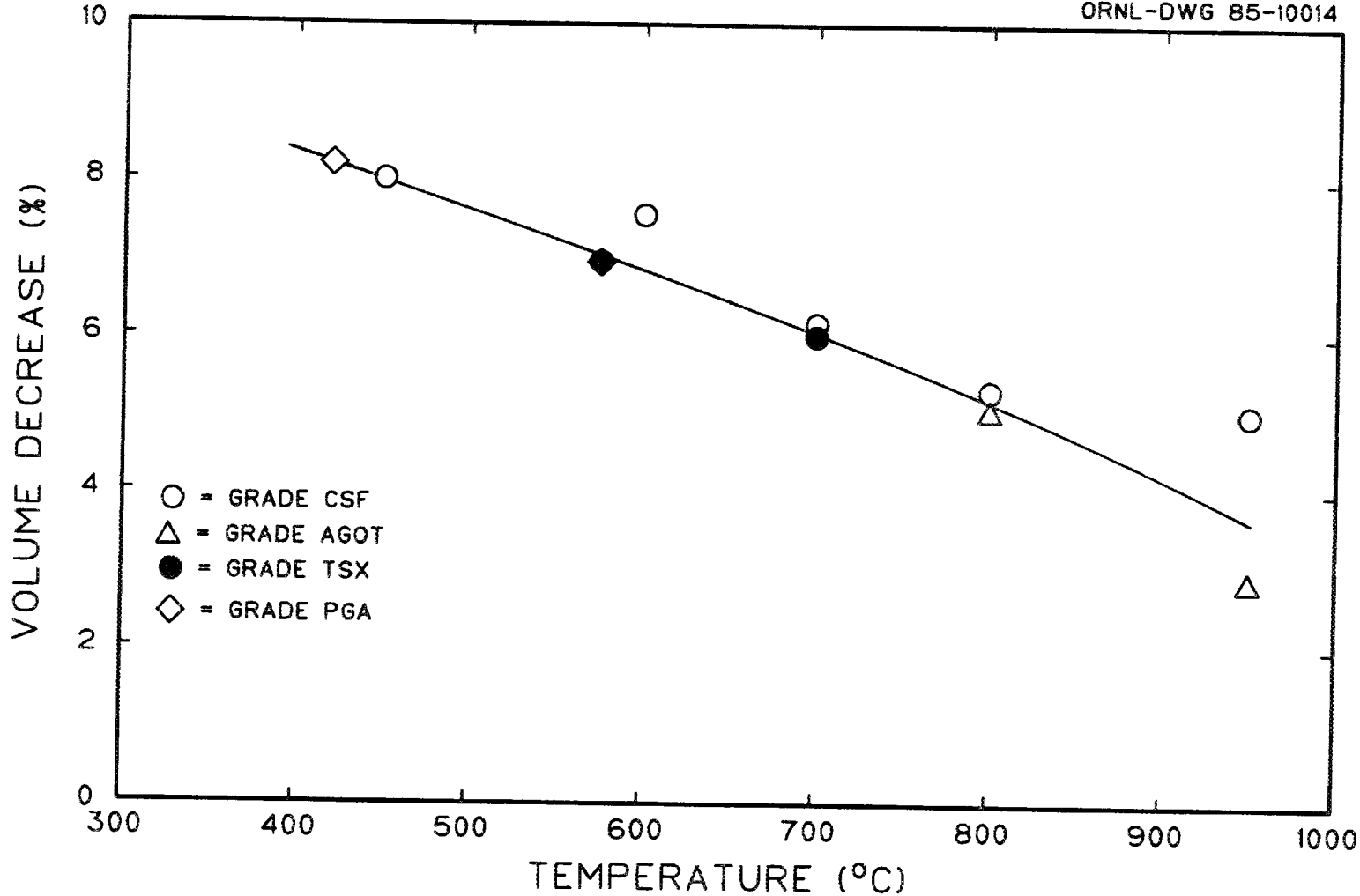


Fig. 1. Maximum densification of acicular graphites by irradiation.

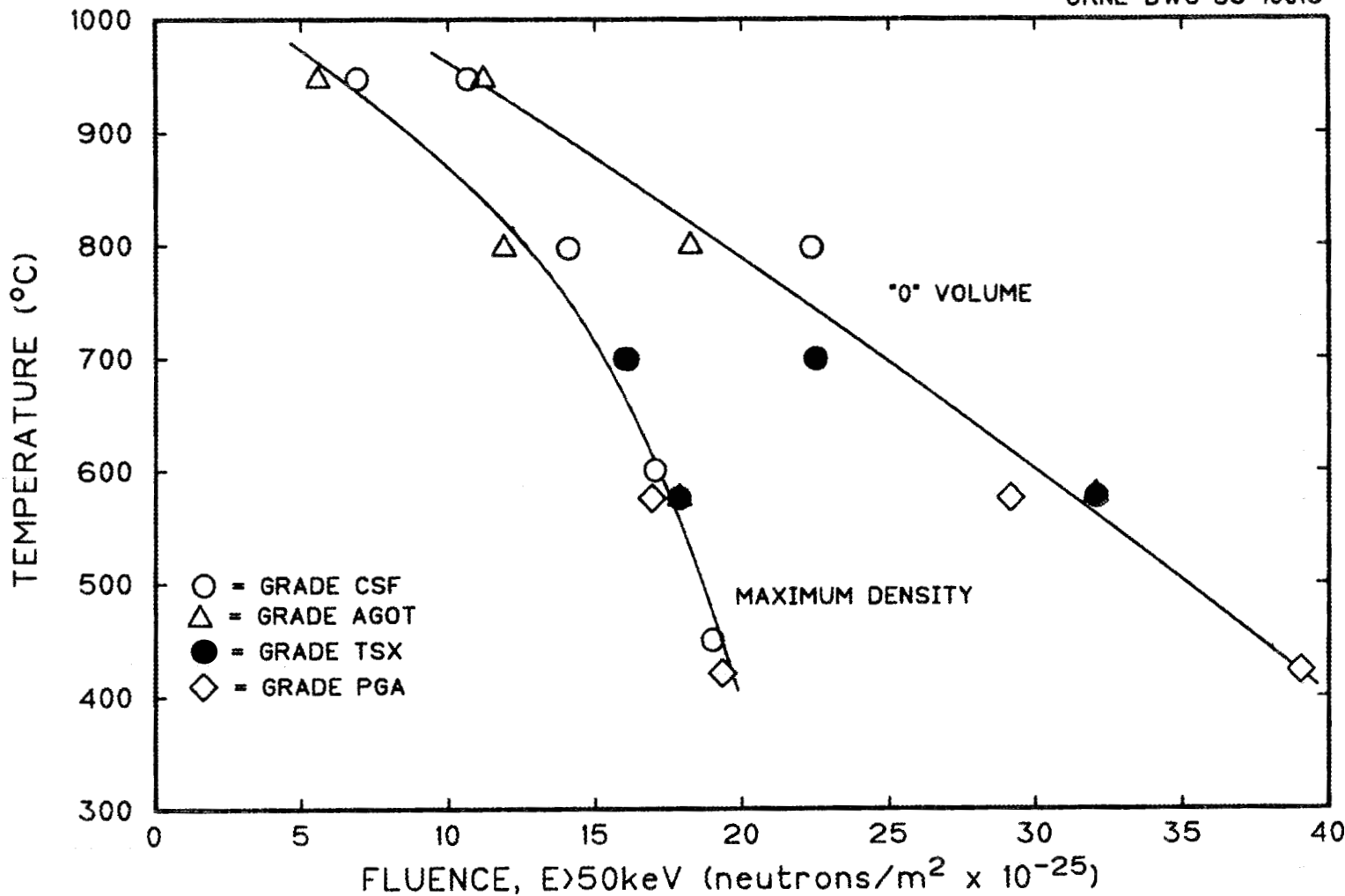


Fig. 2. The fluence required to obtain maximum densification in acicular graphites and that required to return to the original density.

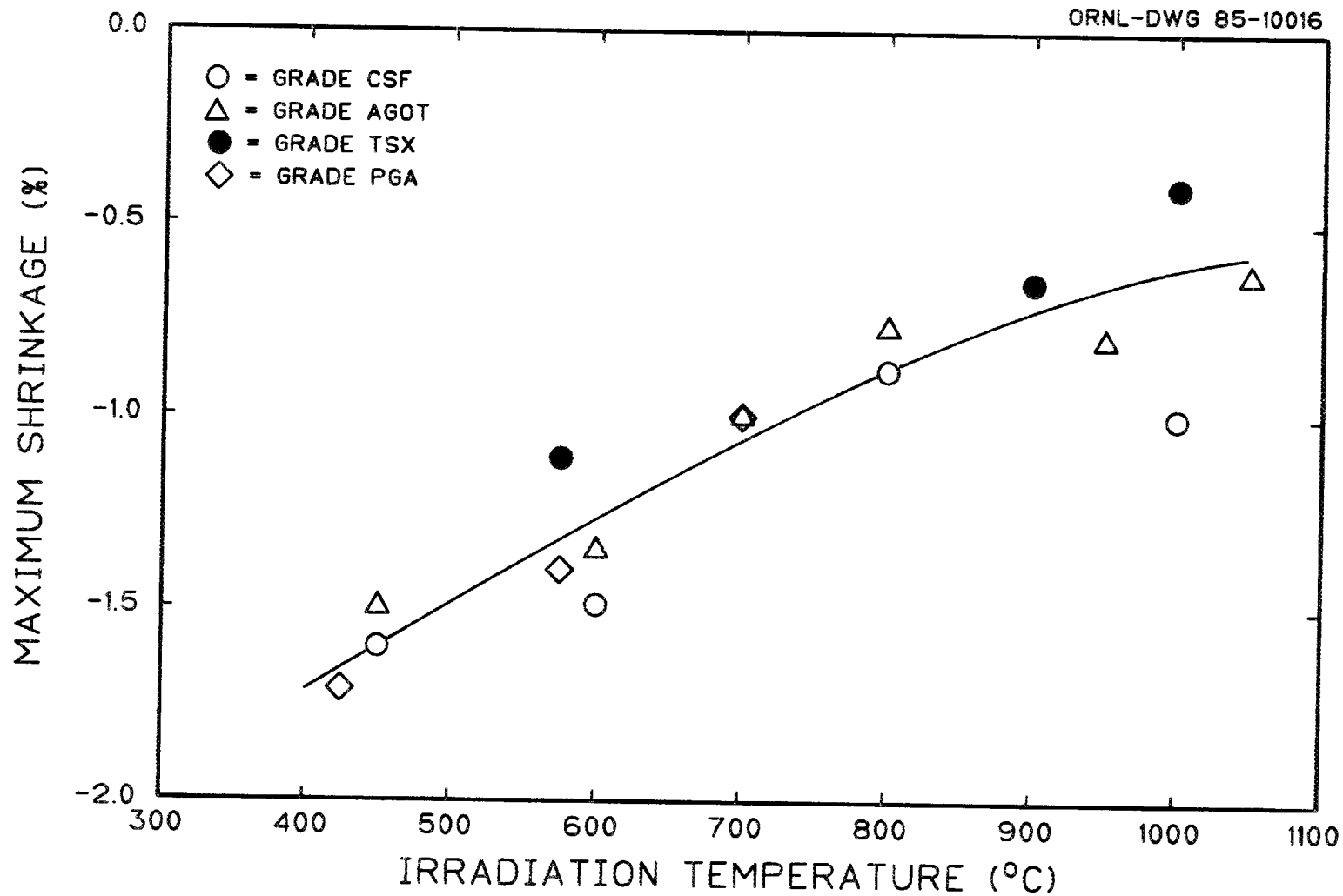


Fig. 3. Maximum shrinkage of acicular graphites in the against-grain direction by irradiation.

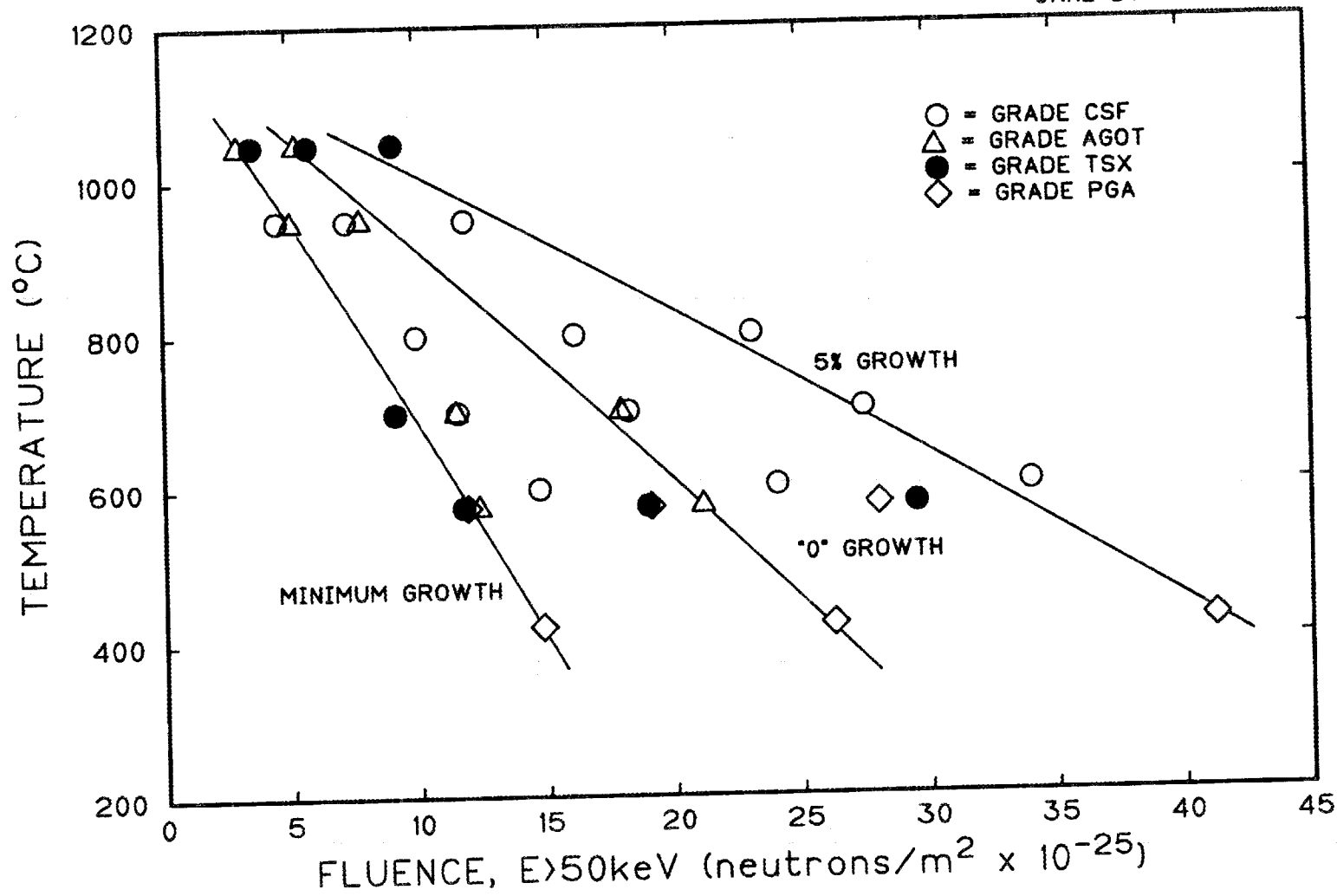


Fig. 4. Fluences required to obtain minimum growth, to return to the original growth, and to obtain 5% growth in the against-grain direction.

points, the transverse growth curves can be roughed in and fitted by the least squares method to the following polynomial expression:

$$\left(\frac{\Delta\lambda}{\lambda_0}\right)_t = A_i + B_i\gamma + C_i\gamma^2 + D_i\gamma^3 \quad , \quad (2)$$

where, in the transverse direction and at temperatures from 400 to 800°C,

$$A_1 = 0.5163 - 9.956 \times 10^{-4} T + 3.82 \times 10^{-7} T^2 \quad ,$$

$$B_1 = -0.2685 + 1.0296 \times 10^{-4} T + 2.7472 \times 10^{-7} T^2 \quad ,$$

$$C_1 = -0.00112 + 6.095 \times 10^{-5} T - 1.156 \times 10^{-7} T^2 \quad ,$$

$$D_1 = 0.00156 - 7.943 \times 10^{-6} T + 1.0604 \times 10^{-8} T^2 \quad ,$$

and where T is temperature in °C and γ is fluence in units of 10^{25} neutrons/m².

The dimensional changes in the axial directions can also be described in a similar manner yielding the following:

$$A_{11} = -0.8396 + 3.389 \times 10^{-3} T - 2.811 \times 10^{-6} T^2 \quad ,$$

$$B_{11} = 0.2508 - 1.348 \times 10^{-3} T + 1.129 \times 10^{-6} T^2 \quad ,$$

$$C_{11} = -4.462 \times 10^{-2} + 9.283 \times 10^{-5} T - 8.136 \times 10^{-8} T^2 \quad ,$$

$$D_{11} = 7.666 \times 10^{-4} - 1.505 \times 10^{-6} T + 1.524 \times 10^{-9} T^2 \quad ,$$

with the same units as above.

Of course, the constants for the higher order terms are fairly small in the axial direction but are included for consistency. The volume change can thus be calculated from the transverse and axial growth data by the expression

$$\frac{\Delta V}{V} = \left(1 + \frac{\Delta\lambda}{\lambda_1}\right)^2 \left(1 + \frac{\Delta\lambda}{\lambda_{11}}\right) - 1 \quad . \quad (3)$$

The results of the growth curve calculations are given in Figs. 5 and 6, and the plots of volume curve calculations are given in Fig. 7.

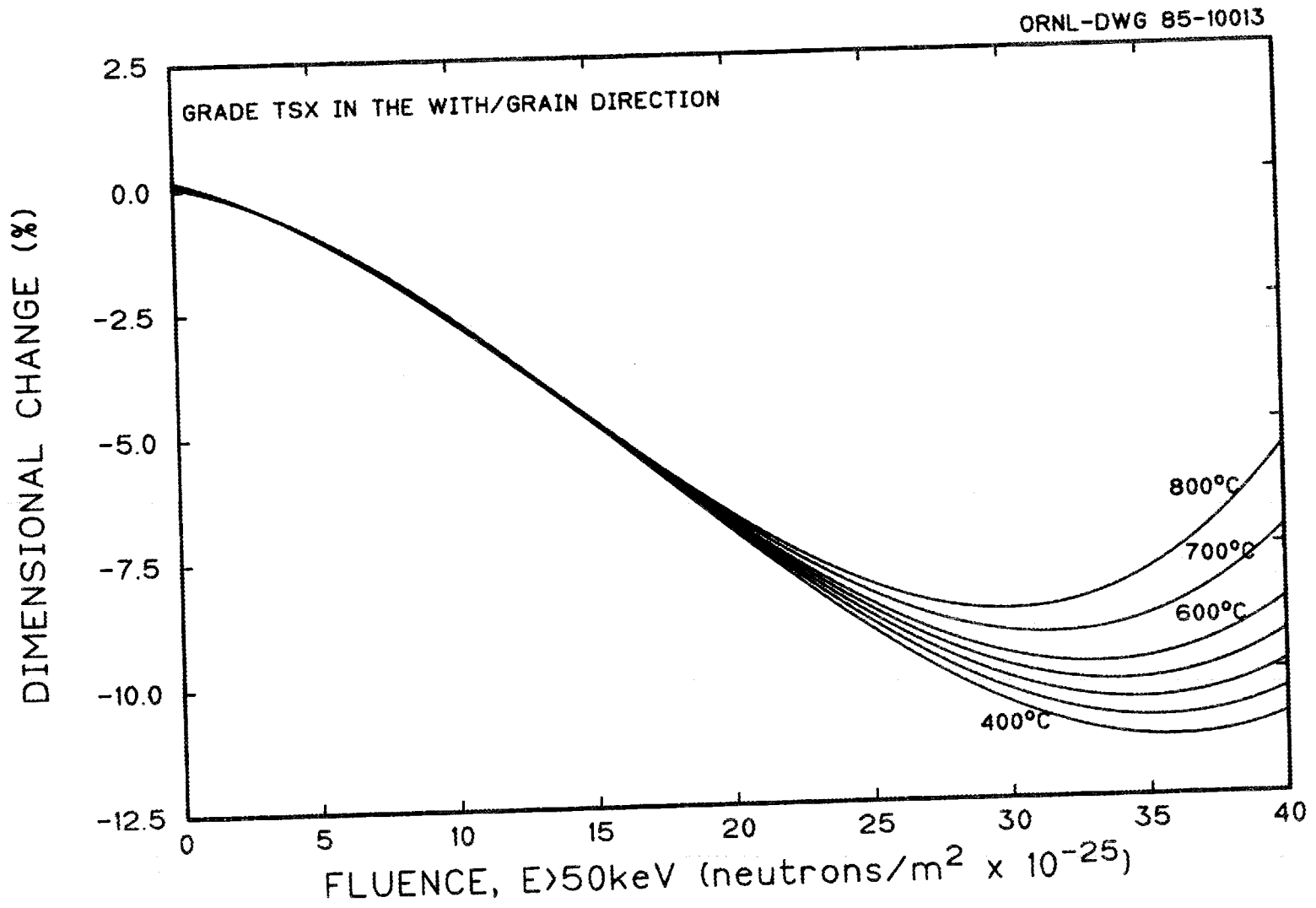


Fig. 5. Calculated dimensional changes of TSX graphite in the with-grain direction.

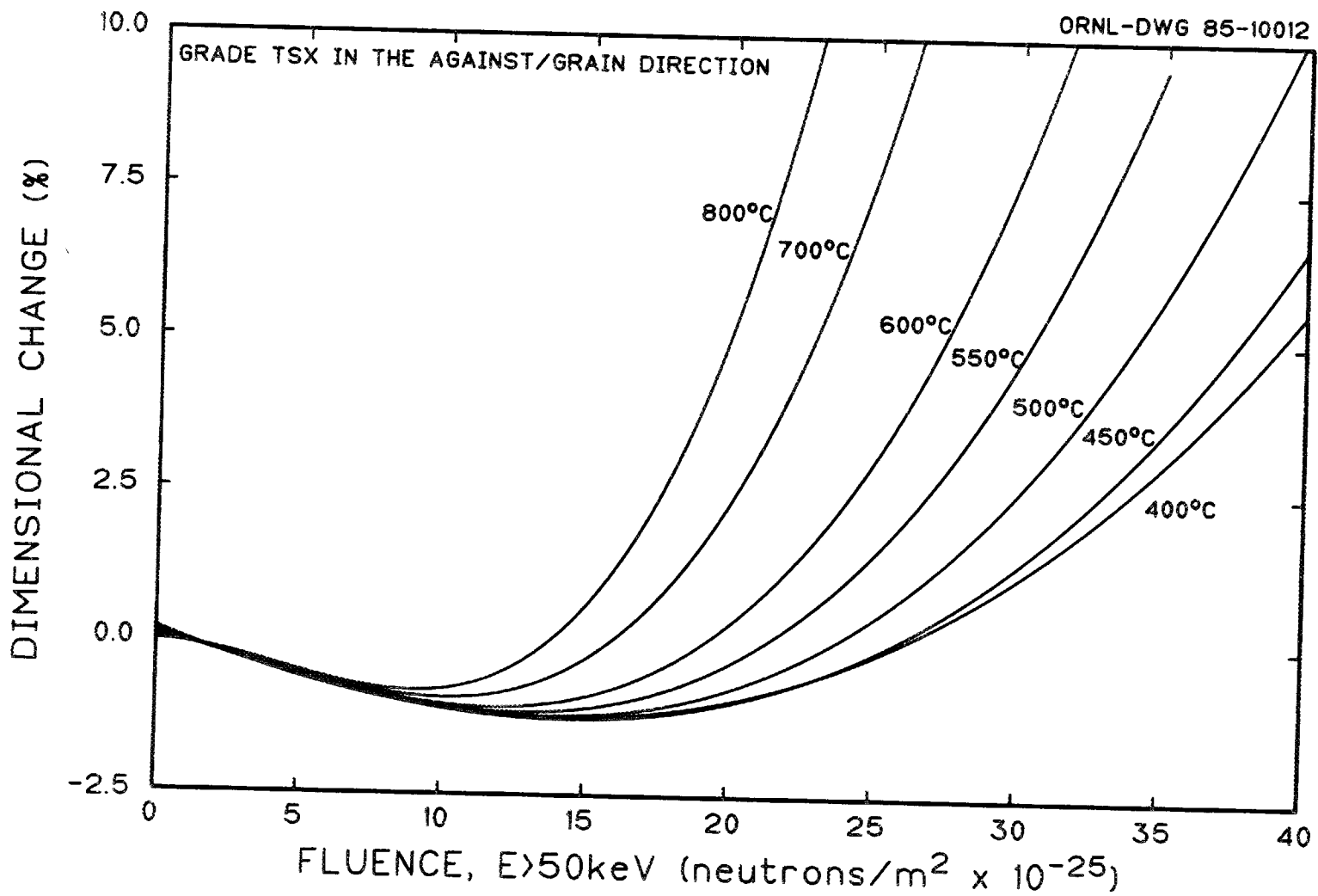


Fig. 6. Calculated dimensional changes of TSX graphite in the against-grain direction.

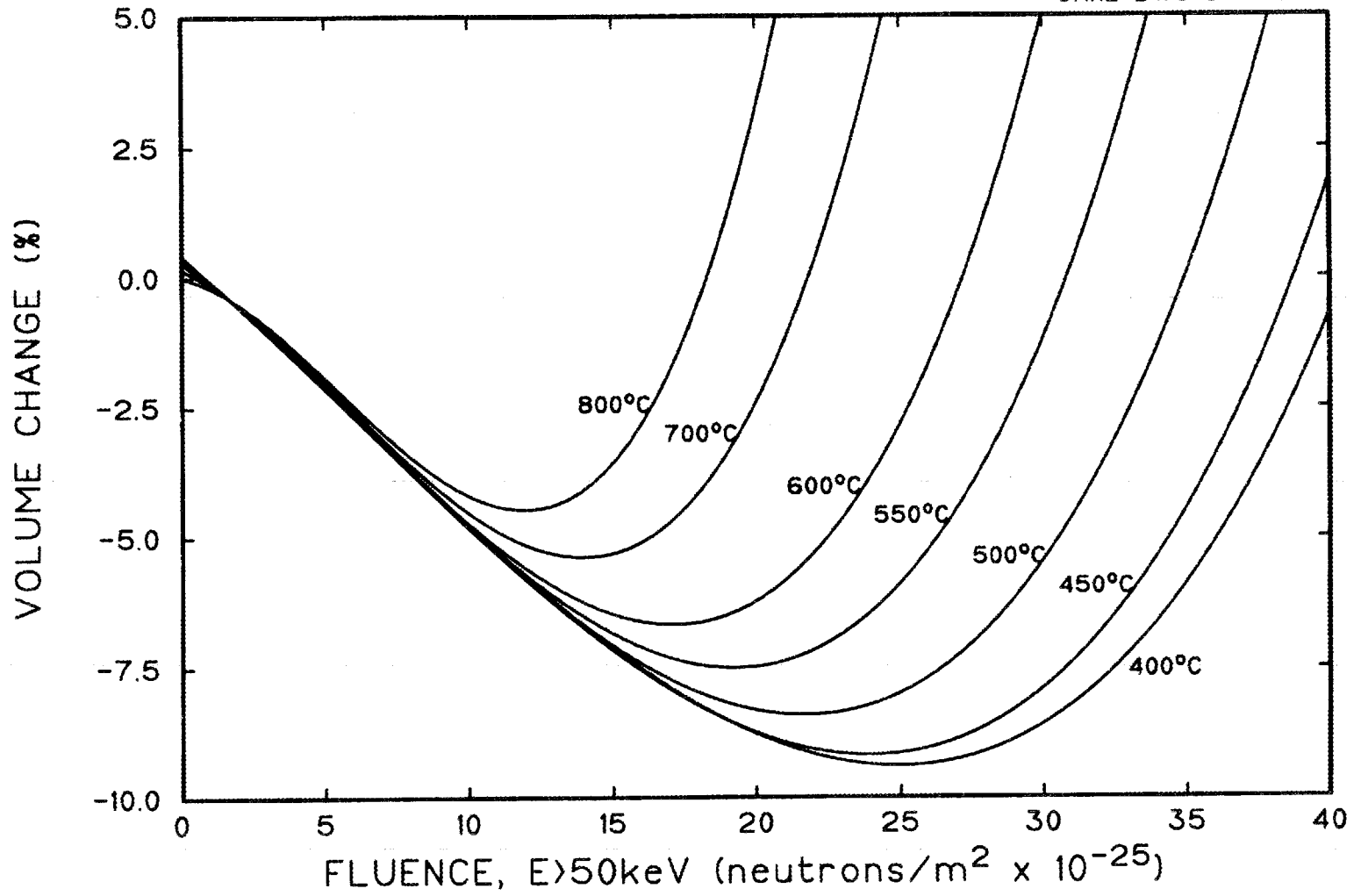


Fig. 7. Calculated volume changes of TSX graphite by irradiation.

Experimental results of samples irradiated in the High Flux Isotope Reactor (HFIR) at Oak Ridge National Laboratory (ORNL) are compared with the calculated data in Figs. 8, 9, and 10. The fit appears to be fairly good and lends credibility to the ability of the above equations to describe the dimensional changes fairly well. These calculations are extremely important in that most of the physical properties and the useful life of the graphite are predicted on the basis of the density changes in the graphite.

FRACTURE STRENGTH

The fracture strength of graphites and most ceramics can be described by the Griffith-Irwin expression:

$$\sigma_f = \left(\frac{G_{Ic} E}{2\pi c} \right)^{1/2} = \frac{K_{Ic}}{(2\pi c)^{1/2}} \quad , \quad (4)$$

where

G_{Ic} = strain energy release rate,

K_{Ic} = fracture toughness,

E = Young's modulus,

c = one-half length of the initial defect size,

σ_f = fracture stress.

Although strength is one measure of the mechanical properties, fracture toughness is probably a better measure under real conditions where stress concentrations are built into the structure. This is particularly true in estimating when the filler-block keys will begin to break. The strength of graphite, or more specifically the change in the probability of fracture, is a very important physical property in the consideration of the useful life of the moderator graphite.

In virtually all fracture tests, the strength has increased initially with irradiation. There is then a leveling off in the strength, followed by an increase as the density of the graphite increases. However, as the

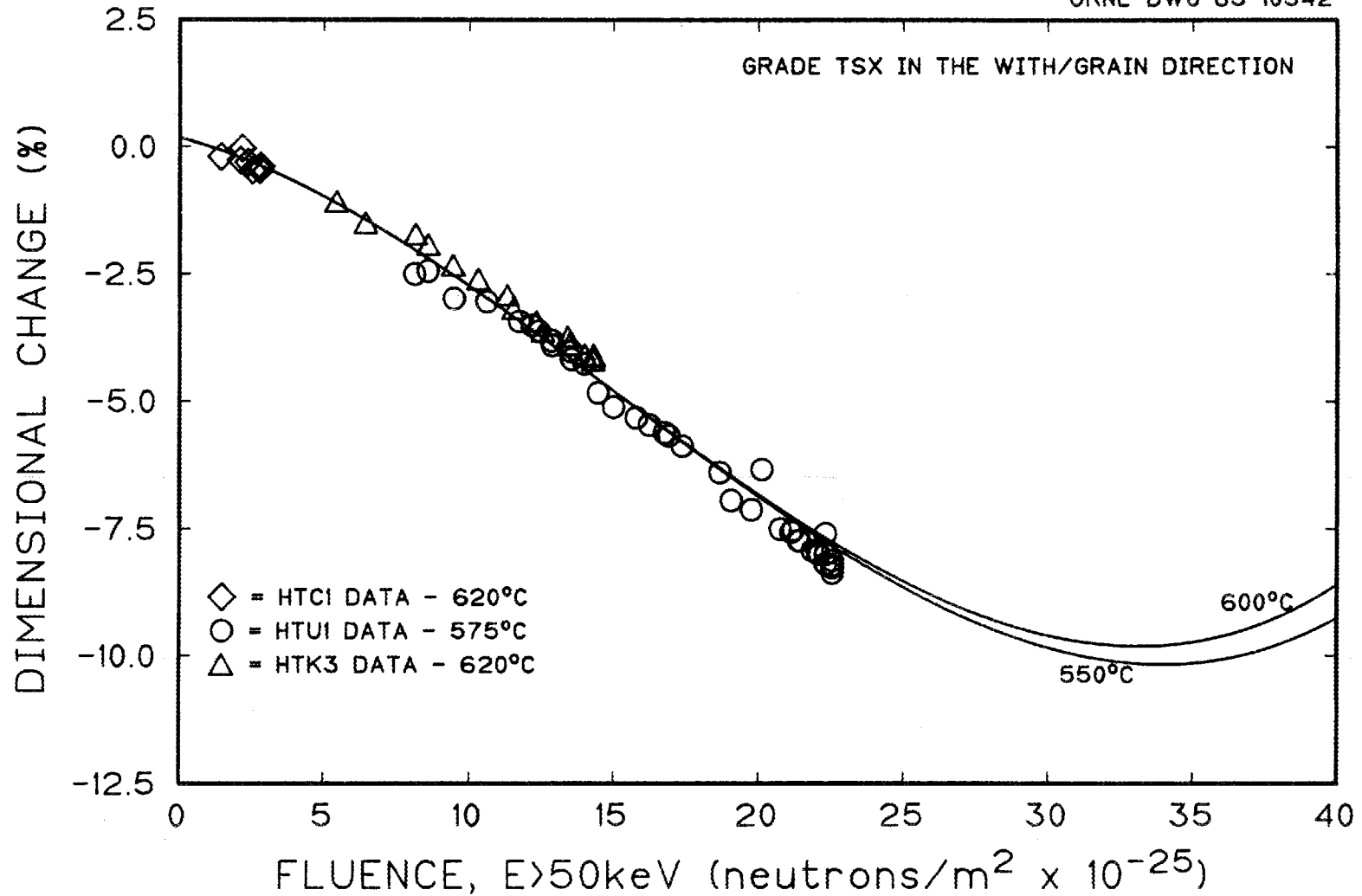


Fig. 8. Calculated dimensional changes in the with-grain direction compared with experimental results of samples irradiated in the High Flux Isotope Reactor (HFIR).

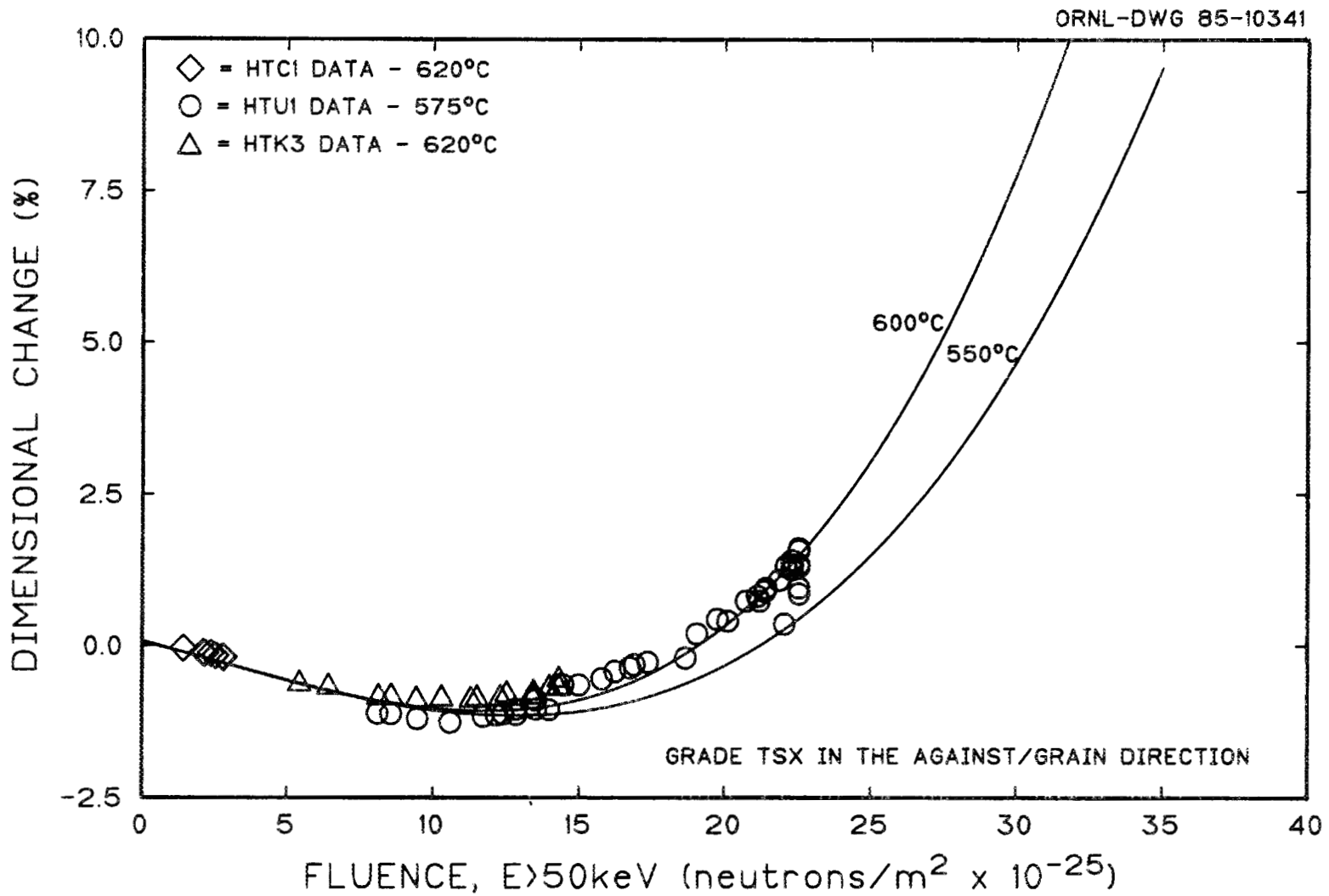


Fig. 9. Calculated dimensional changes in the against-grain direction compared with experimental results of sample irradiated in the HFIR.

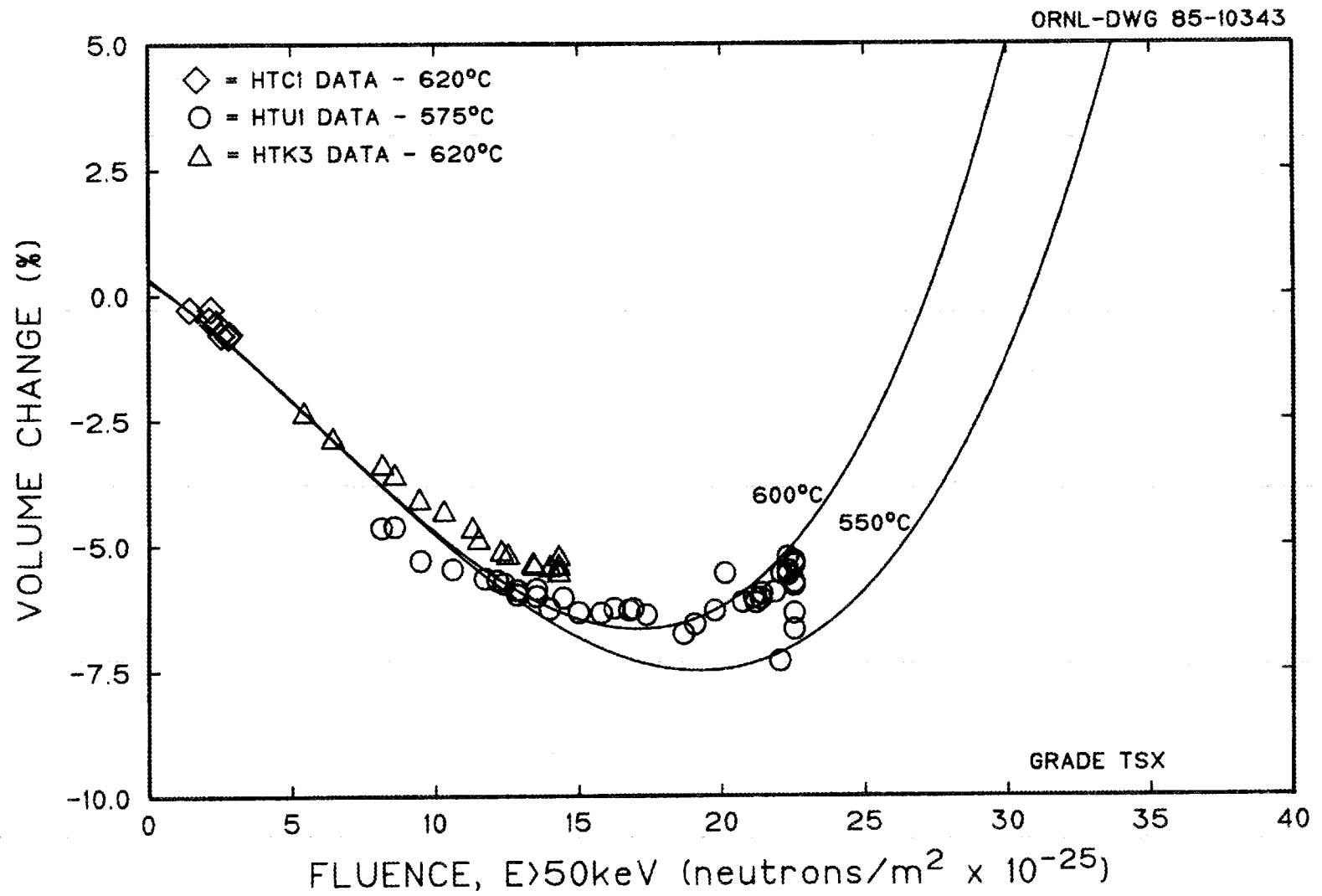


Fig. 10. Calculated volume changes compared with experimental results of samples irradiated in the HFIR.

maximum density is achieved and the graphite begins to expand, the strength begins to decrease. It has been found that, as the graphite expands back to its original volume, the strength is reduced but is still 30 to 50% stronger than the initial unirradiated strength. This type of behavior is shown in Figs. 11 and 12 for a German-grade ASR-1R graphite.¹⁶ Figure 13 is a comparison of the initial unirradiated strength with the strength after irradiation to zero volume change. Although the graphite maintains some degree of integrity to volume expansions of 10 to 20%, the strength may fall to less than 50% of the initial strength; therefore, it has been a practice to consider the useful life of graphite under irradiation as that fluence which causes the graphite to return to its original density. The fracture strength of TSX graphite irradiated in the HFIR is shown in Fig. 14.

However, although the fracture strength increases to values of almost twice the initial strength, our studies have shown that the fracture toughness increases only a slight amount. Also, as the maximum density is reached, the fracture toughness begins to decrease. The decrease in fracture toughness with fluence is not so severe as to change the definition of useful life by volume change. In the case of filler-block key fracture, credit should not be taken for the increased fracture strength of TSX by irradiation.

The results of the fracture toughness studies in progress at ORNL also permit a description of the structural changes that occur during irradiation that will affect other properties. The slight increase in fracture toughness in contrast to the large increase in strength indicates that the strength increase is the result of an increased modulus of elasticity and a reduced critical defect size. The strain-energy release rate, G_{Ic} , or the energy to create new surfaces, is actually reduced by irradiation throughout its life. The reduction of G_{Ic} and the increased surface area produced by irradiation are a result of a new flaw structure, much smaller than the critical defect size, that is created by the differential growth. This flaw structure is also oriented normal to the layer planes in contrast to the original predominantly parallel flaw structure. These new flaws increase in number but have not been observed

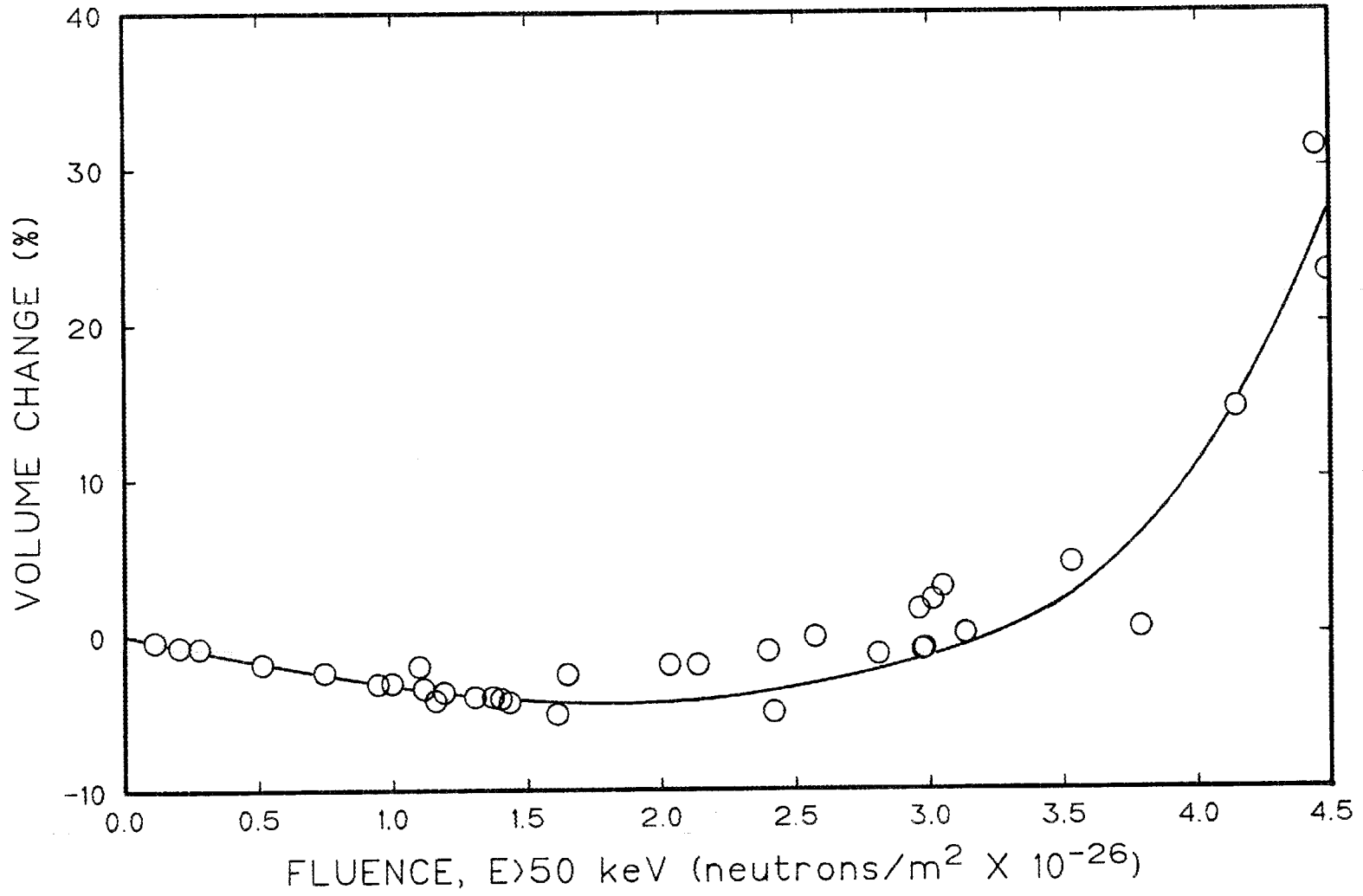


Fig. 11. Effect of irradiation on volume changes in grade ASR-1R graphite at 620°C.

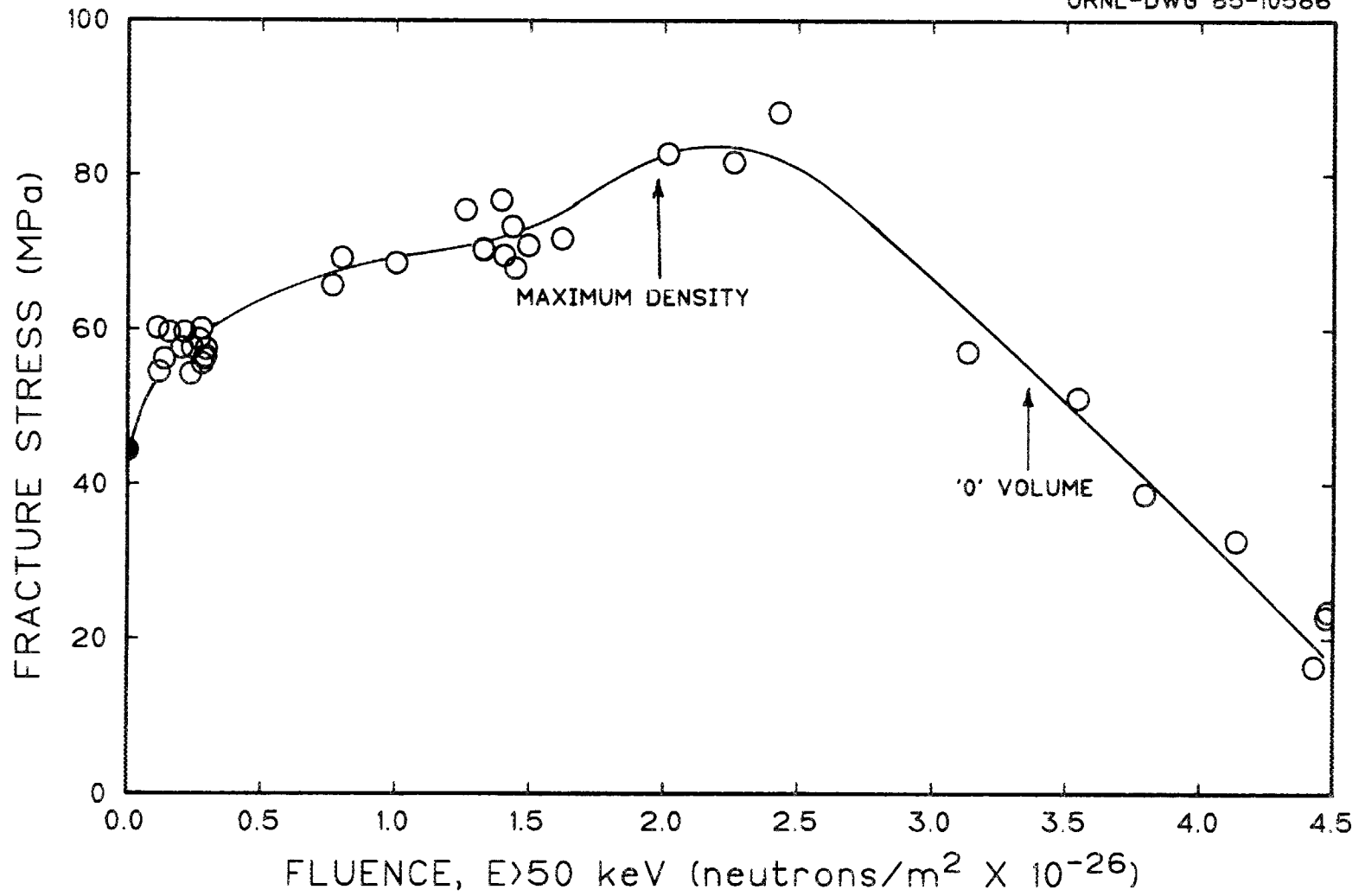


Fig. 12. Effect of irradiation on the fracture strength of grade ASR-1R graphite at 620°C.

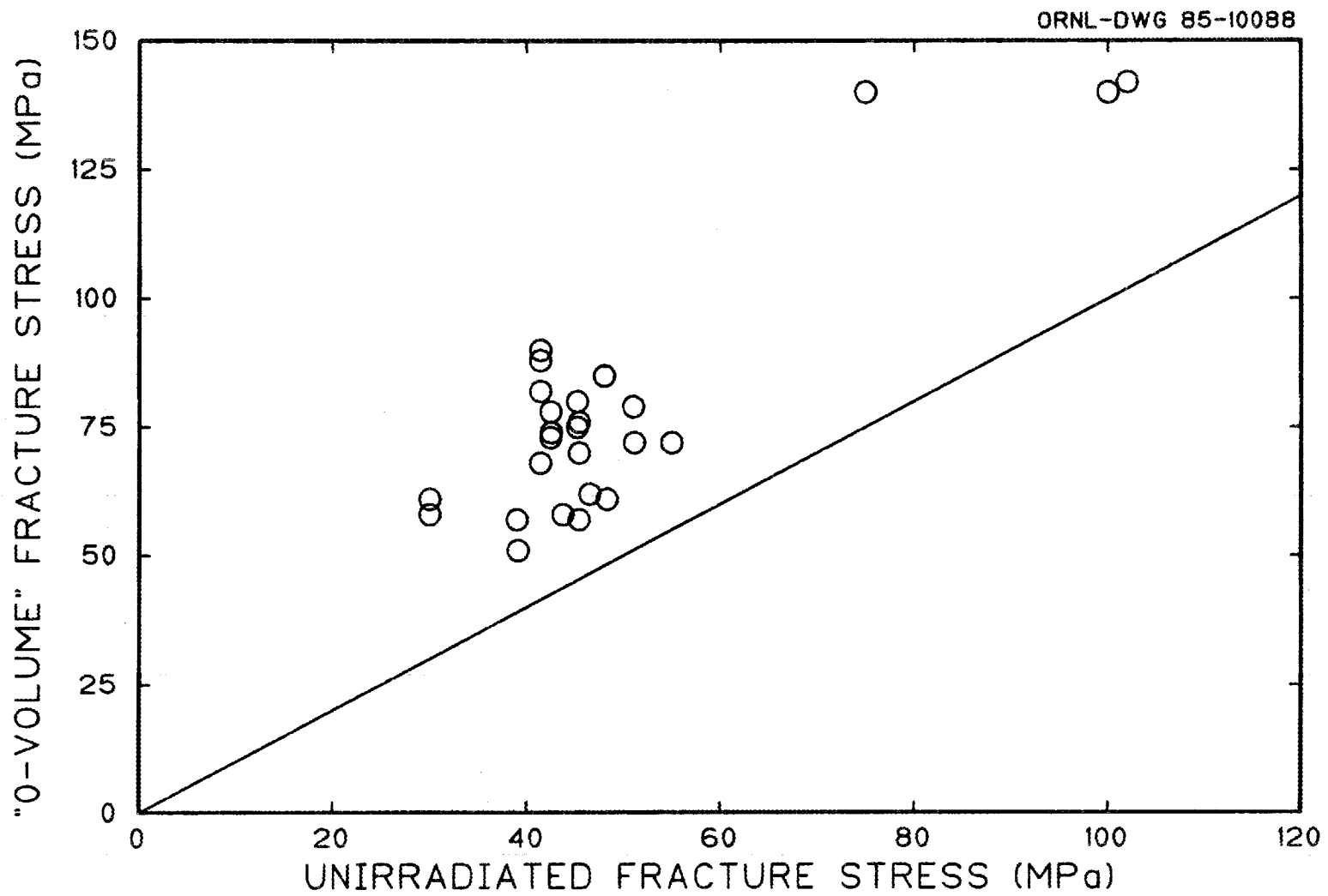


Fig. 13. Fracture strength of various grades of graphite at the end of expected life.

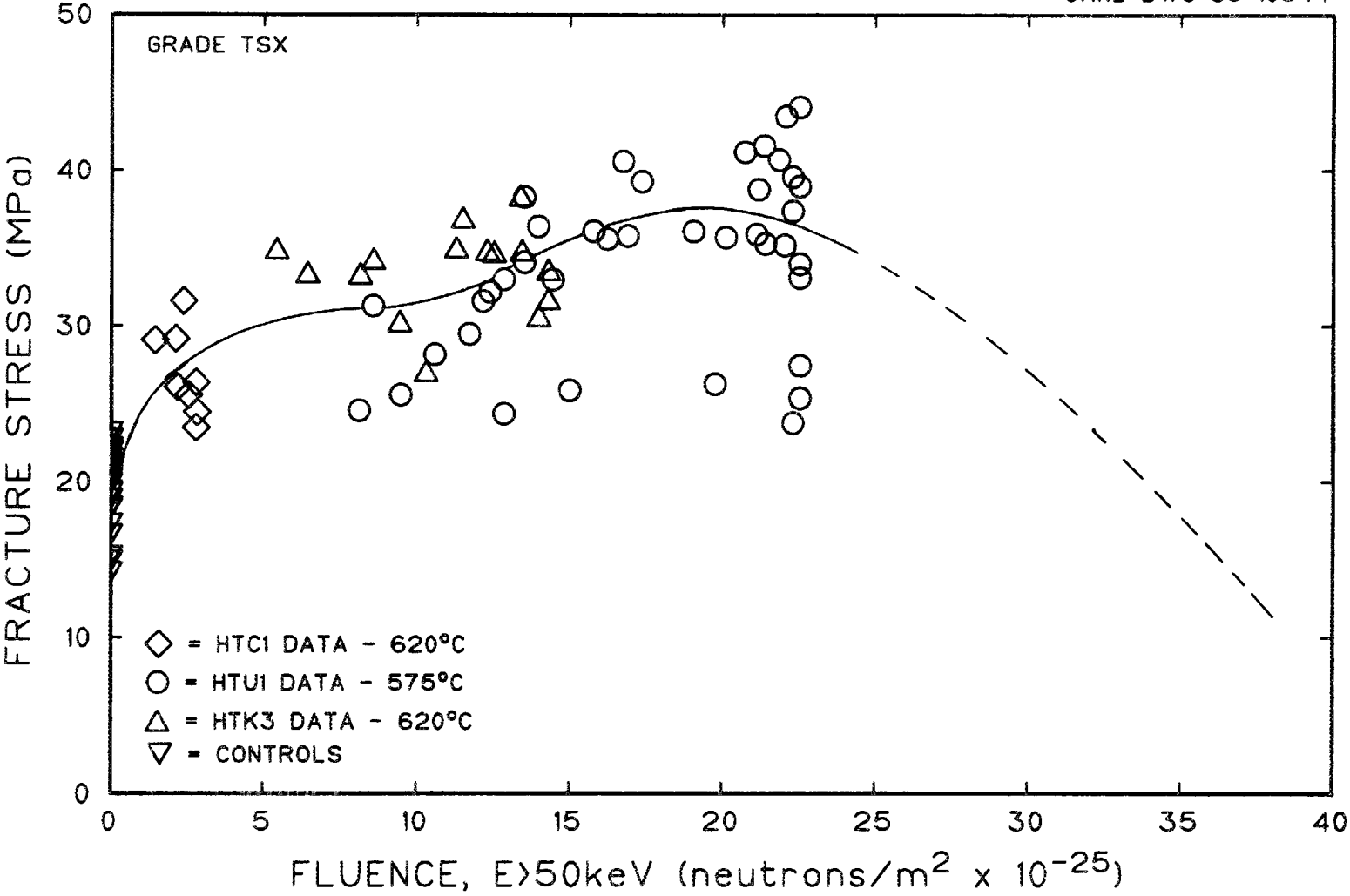


Fig. 14. Brittle-ring fracture strength of TSX graphite irradiated at 575°C in the HFIR.

to increase to a size greater than the reduced critical flaw size of the original unirradiated structure. The strength is almost totally maintained by the increased Young's modulus; as the density decreases, the modulus decreases and the associated strength decreases.

MODULUS OF ELASTICITY

The modulus of elasticity increases with irradiation because of the pinning of dislocations by vacancy clusters within the lattice. Thus, the modulus of elasticity increases very rapidly with irradiation, tends to level out, and then increases again as density increases; as the maximum density is obtained the modulus begins to decrease. The effect of irradiation temperature on the overall behavior is not very great and depends mainly on the effect of temperature on density changes. The modulus of TSX graphite is shown in Fig. 15 with extrapolated values based on density changes at 575°C.

THERMAL CONDUCTIVITY

An excellent review of the thermal conductivity of graphite, consolidating most of the available data, has been written by Price.¹⁷ Initially, the conductivity is rapidly reduced and levels off to a more or less constant value. This initial loss of conductivity is due to sub-microscopic clusters of vacancies in the lattice in contrast with the interstitial loops and collapsed vacancy lines responsible for dimensional changes. The saturation of vacancies remains essentially constant and without additional structural changes; the conductivity also remains constant. However, as mentioned in the sections on mechanical properties, internal changes occur as a result of the anisotropic crystallite growth. As the graphite densifies and reduces the overall porosity, the conductivity should increase slightly. This increase is countered by the added resistance of the new pore generation. The new pore structure, normal to the basal planes, significantly increases the boundary resistance. After maximum densification, the volume begins to expand and the conductivity

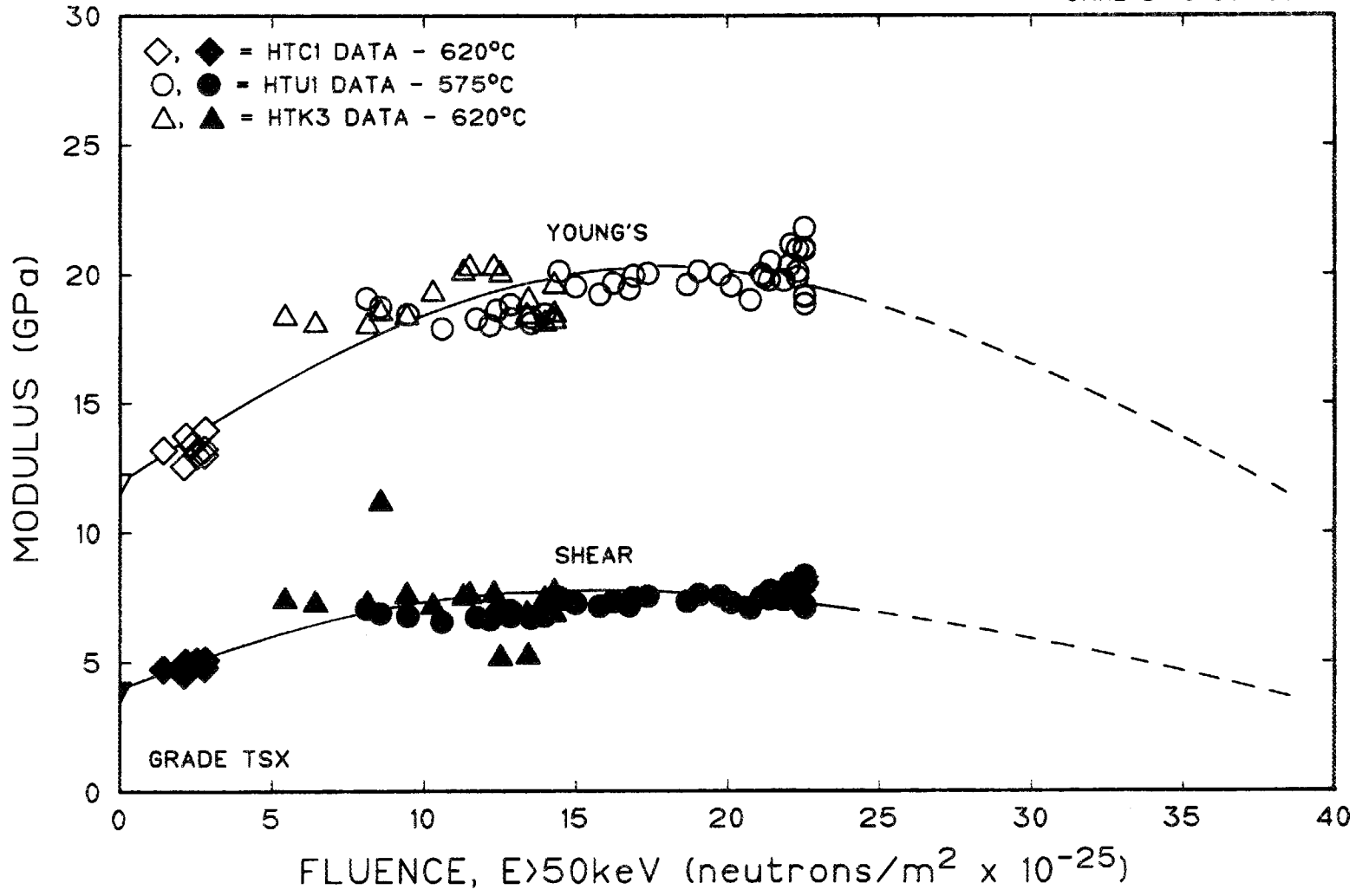


Fig. 15. Modulus of elasticity of TSX graphite irradiated at 575°C in the HFIR.

begins to decrease. By following the consolidated results of Price (given in Appendix A) and the electrical resistivity data for TSX material irradiated in the HFIR (given in Fig. 16), the expected thermal conductivity of material irradiated in the N-Reactor can be extrapolated as shown in Figs. 17 and 18.

COEFFICIENTS OF THERMAL EXPANSION

Initially, the coefficient of thermal expansion (CTE) is only moderately affected by irradiation in the with-grain direction; however, the CTE in the against-grain direction increases by about 40 to 50%. This increase is due to the differential anisotropic growth closing the defect structure parallel to the basal planes that reduce the CTE. The CTE then remains essentially constant until the maximum density is obtained; then the CTE in both directions begins to increase. The last increase is a result of the loss of continuity in the α -axis by the generation of the new pore structure normal to the basal planes.

It must be recognized that the measurements have been made after irradiation and only to a temperature below the actual irradiation temperature. As the graphite is cooled from the irradiation temperature, the anisotropic shrinkage actually recreates the defect structure parallel to the layer planes, reducing the CTE even if the irradiation had completely closed the defect structure during irradiation. Thus, if a heavily irradiated graphite is heated to temperatures above the irradiation temperature, the CTE changes abruptly at the irradiation temperature as shown in Fig. 19 for grade H451 graphite. This change is of concern only if temperature increases larger than 50 to 100°C are encountered in operation, which is unlikely. The CTE of TSX as measured to the irradiation temperature is given in Fig. 20 with extrapolations made to useful life.

IRRADIATION CREEP

Graphite experiences a time-dependent plastic deformation under stress and irradiation. This topic has been reviewed recently by Price¹⁸

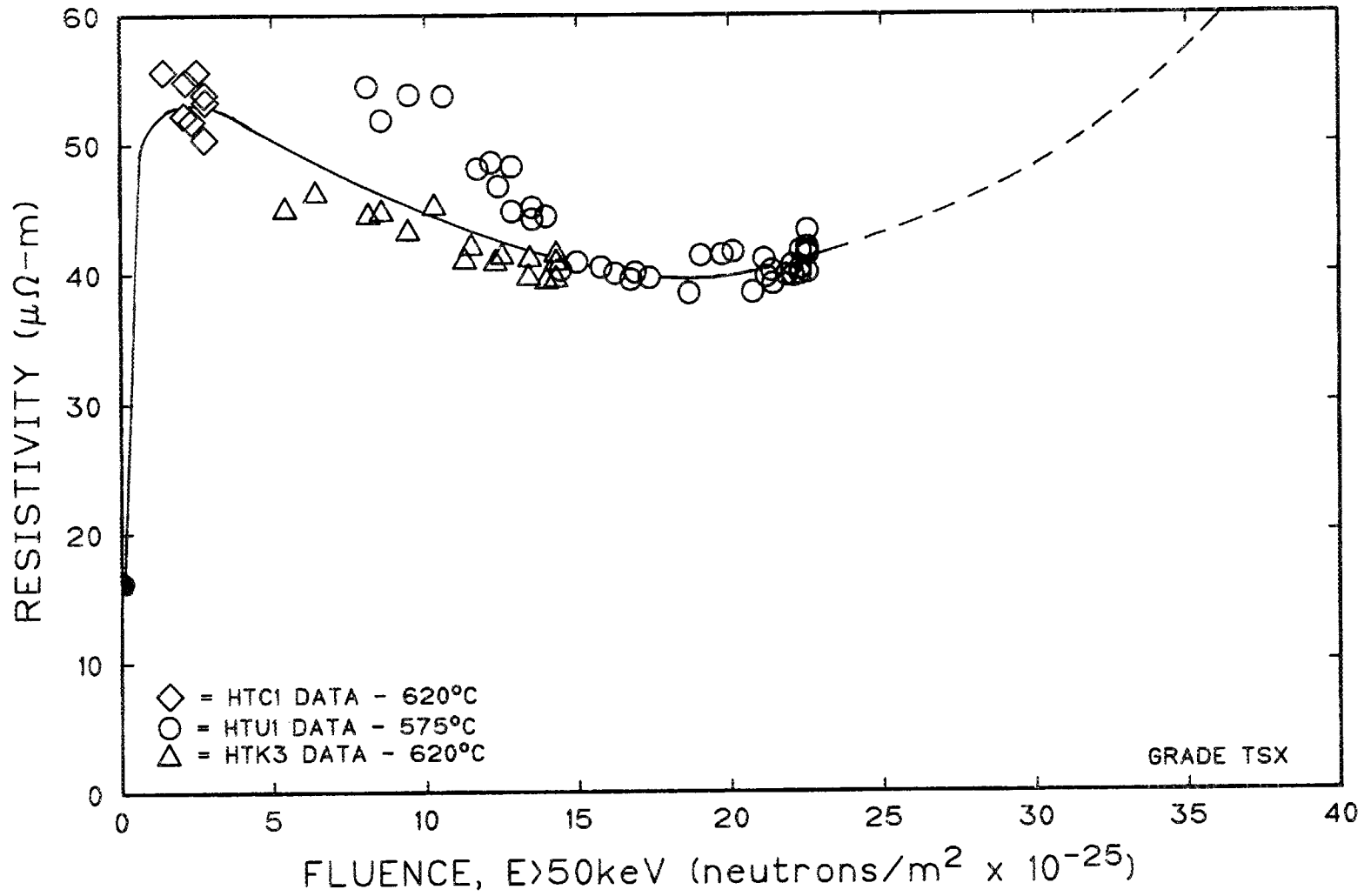


Fig. 16. Electrical resistivity of TSX graphite irradiated at 575°C in the HFIR.

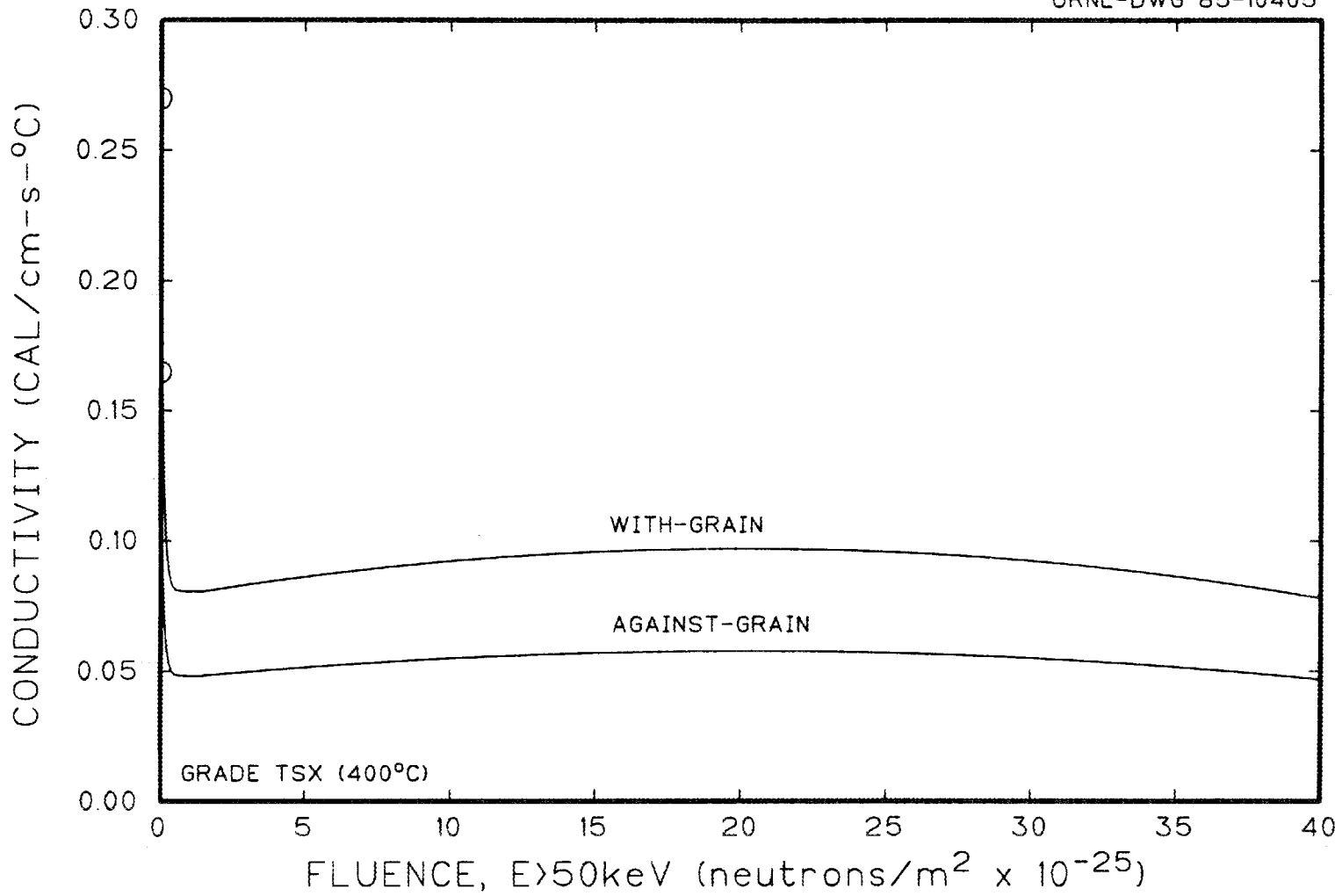


Fig. 17. Estimated 400°C thermal conductivity of TSX graphite irradiated at 400°C.

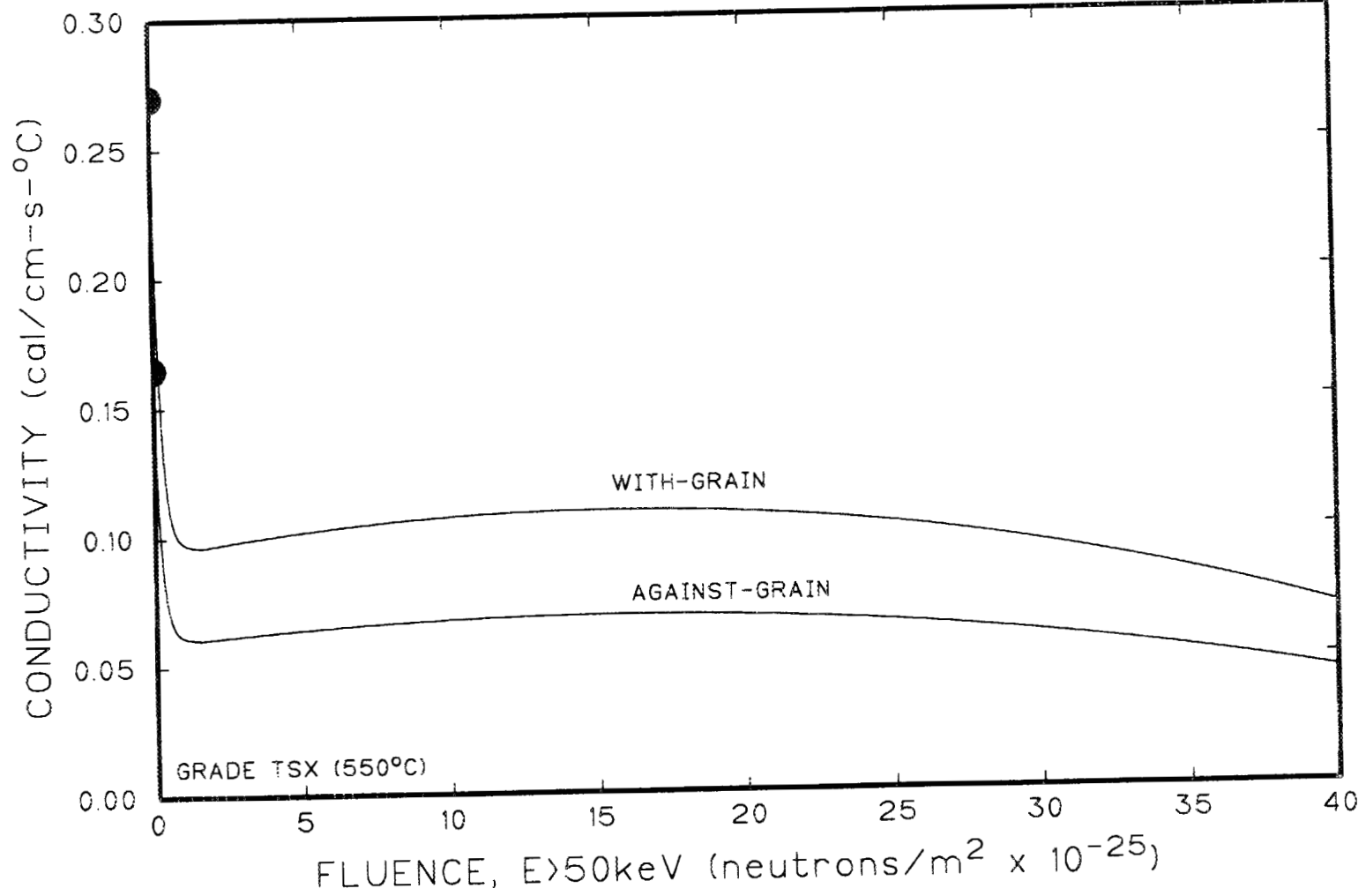


Fig. 18. Estimated 550°C thermal conductivity of TSX graphite irradiated at 550°C.

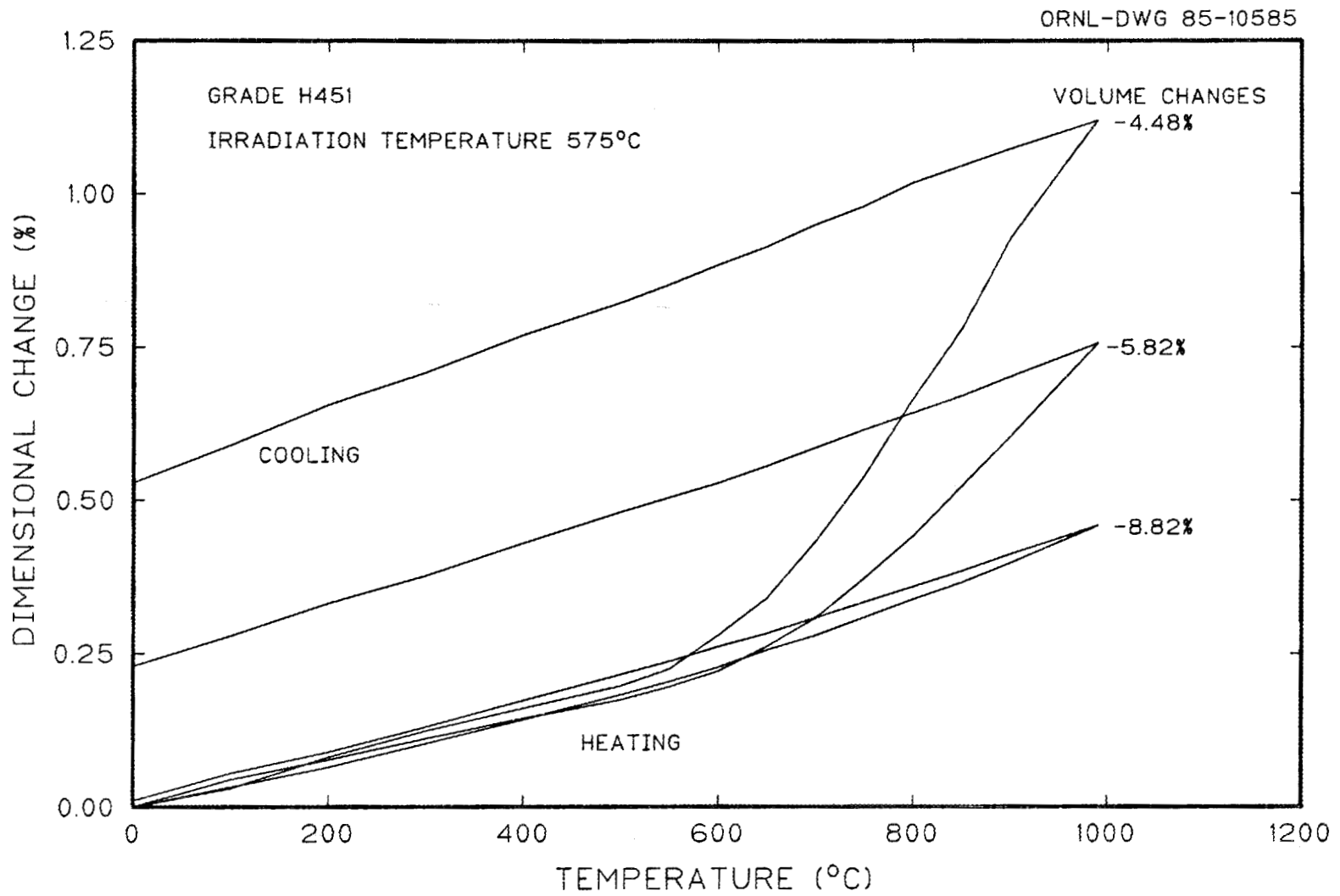


Fig. 19. Thermal expansion of grade H451 graphite heated to above the irradiation temperature.

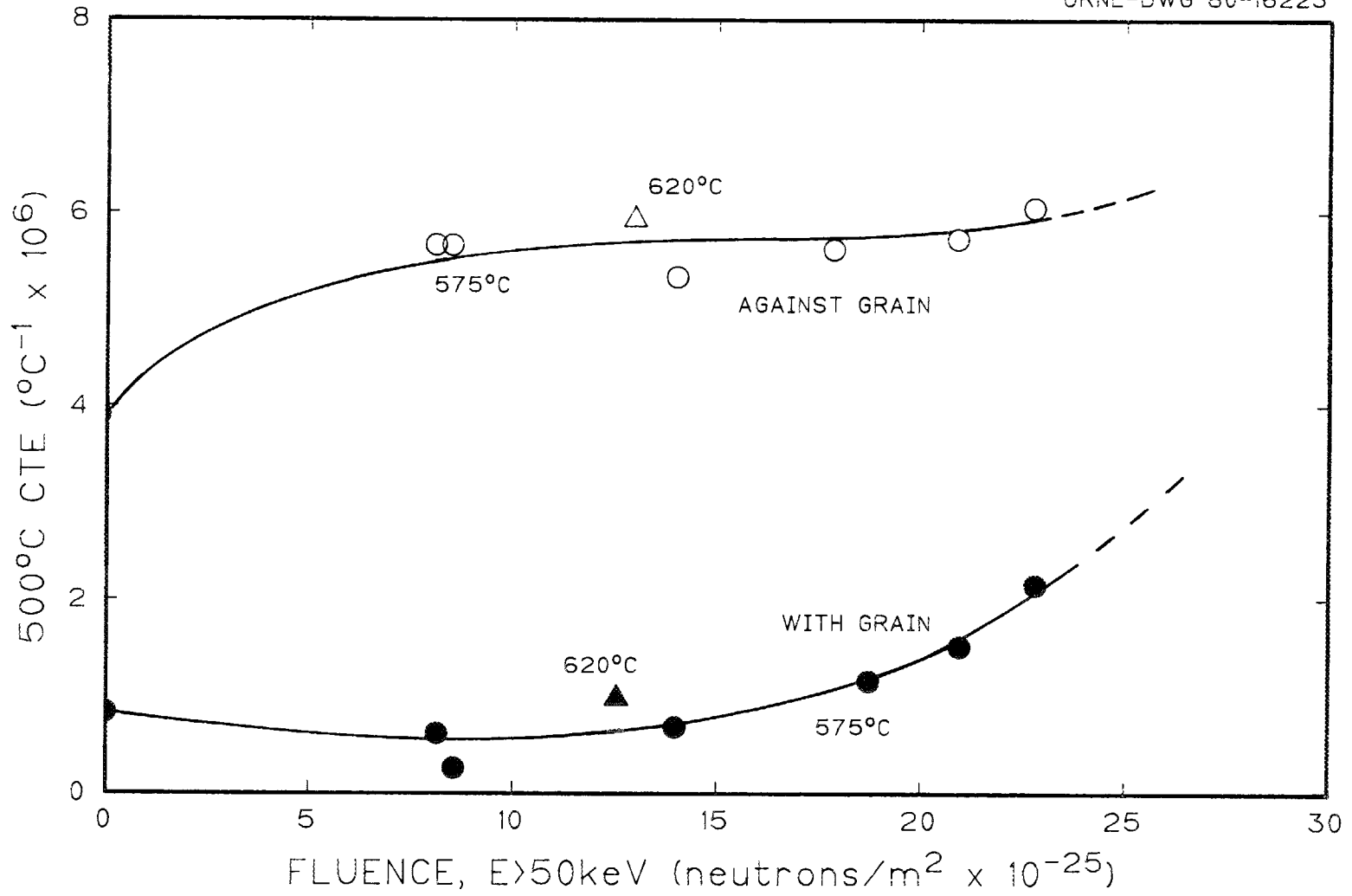


Fig. 20. Coefficient of thermal expansion of TSX graphite irradiated at 575°C.

and thus will not be discussed in detail. It is fairly well accepted that the creep of graphite at a single temperature is related to the elastic constants of the graphite; that is, the creep rate is inversely proportional to Young's modulus. Therefore, it is possible to estimate the creep rate of TSX graphite from other creep test results. There does seem to be some evidence of a slightly higher creep rate in tension than in compression; however, previous creep tests in bending are in fairly good agreement with compression tests on like materials. The level of confidence is not large enough to consider a difference in tension and compression. There is a real decreasing creep rate with fluence in both tension and compression. Recent German creep tests at Petten¹⁹ to large fluences indicate a slightly decreasing creep rate until maximum densification, followed by a slight increase. The most recent results¹⁹ are given in Figs. 21 and 22 for grade ATR-2E, a German moderator-grade graphite. The data on secondary creep coefficient, weighting the ORNL compression creep tests and the Petten creep tests more heavily, yield the following value for uniaxial results:

$$\dot{\epsilon} = \frac{c}{E} \sigma \quad (5)$$

with

$$c = [1.93 - 3.78 \times 10^{-3} T + 4.25 \times 10^{-6} T^2] \times 10^{-25} \quad (6)$$

This value is slightly lower than that used by Price to better take into account the decreasing creep rate with fluence.

There have been no creep studies of graphite under multiaxial loading. The failure surface determined from multiaxial fracture studies is of no help in that essentially no yielding or plastic flow in the normal context occurs before fracture. We are left to use models shown to be applicable for other anisotropic materials such as zirconium alloys. The plastic potential as defined by Hu²⁰

$$f = \bar{\sigma}^2 = \alpha_{12}(\sigma_{11} - \sigma_{22})^2 + \alpha_{23}(\sigma_{22} - \sigma_{33})^2 + \alpha_{31}(\sigma_{33} - \sigma_{11})^2 \quad (7)$$

gives the Levy-Mises equations by analogy

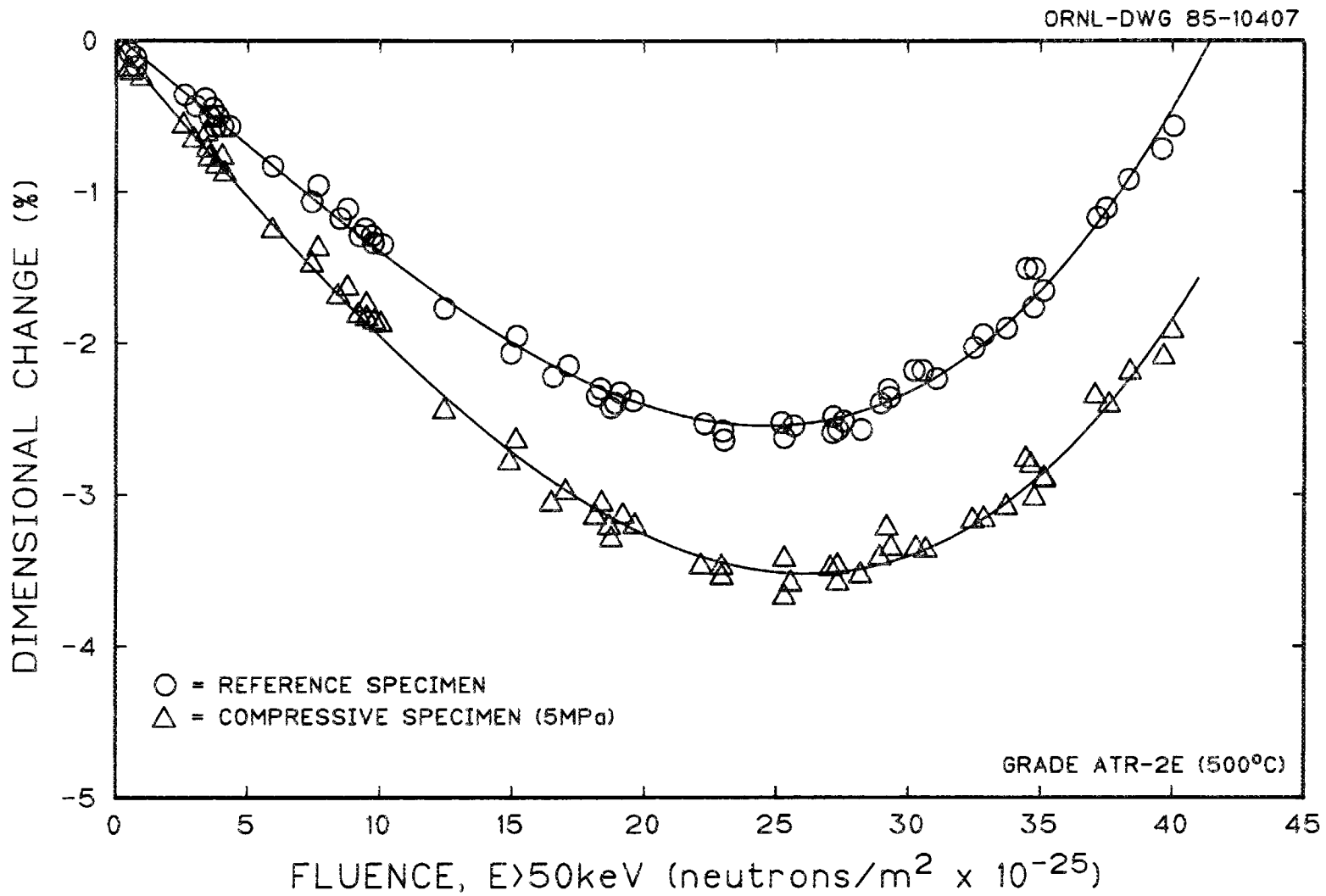


Fig. 21. Dimensional changes of grade ATR-2E graphite at 500°C under compressed load.

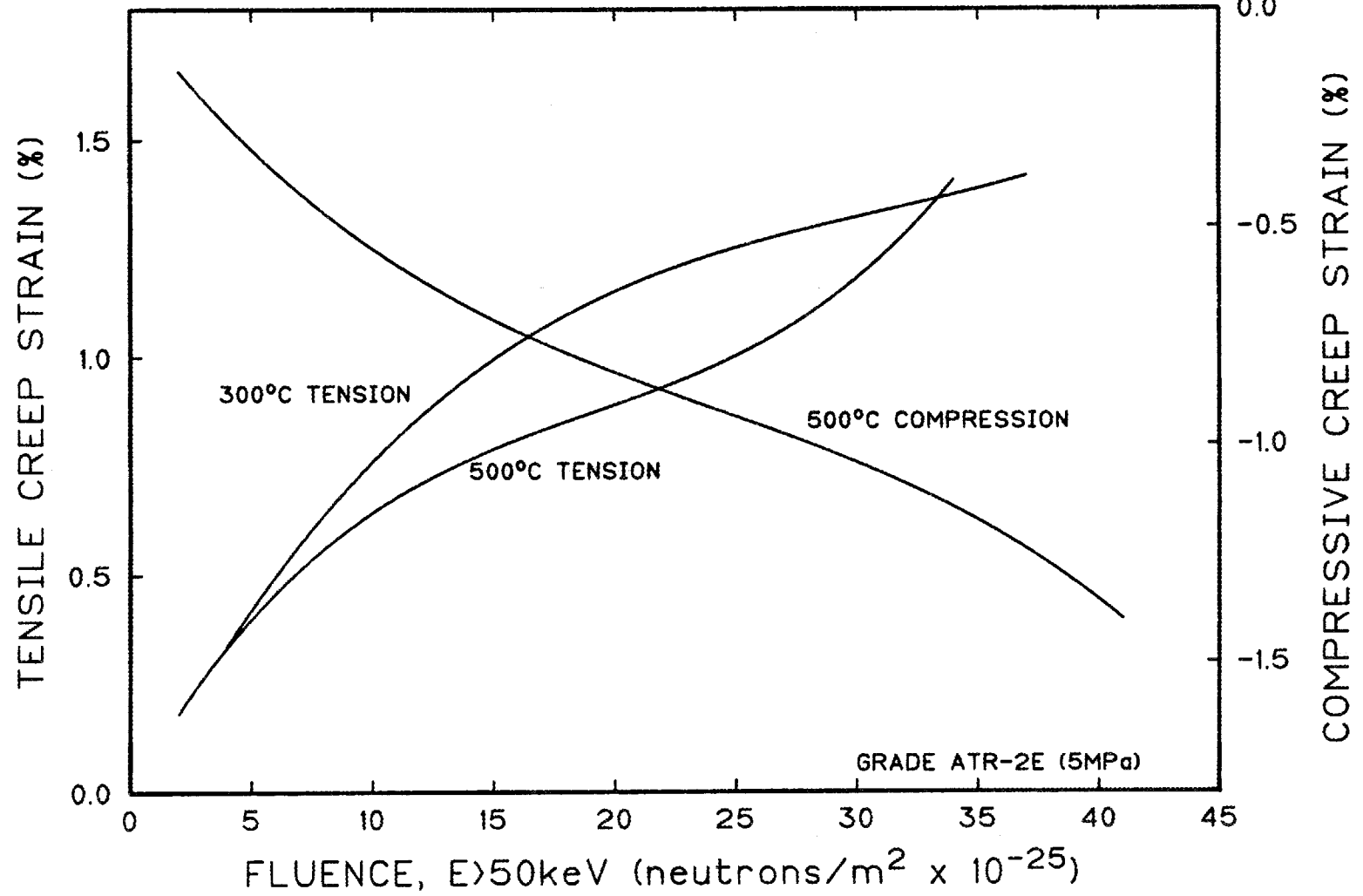


Fig. 22. Creep strains of grade ATR-2E graphite under 5 MPa load.

$$\dot{\varepsilon}_{11} = \dot{\lambda}(\alpha_{11}\sigma_{11} - \alpha_{12}\sigma_{22} - \alpha_{31}\sigma_{33})$$

$$\dot{\varepsilon}_{22} = \dot{\lambda}(\alpha_{22}\sigma_{22} - \alpha_{23}\sigma_{33} - \alpha_{12}\sigma_{11})$$

$$\dot{\varepsilon}_{33} = \dot{\lambda}(\alpha_{33}\sigma_{33} - \alpha_{31}\sigma_{11} - \alpha_{23}\sigma_{22})$$

where

$$\alpha_{11} = \alpha_{12} + \alpha_{31}$$

$$\alpha_{22} = \alpha_{23} + \alpha_{12}$$

$$\alpha_{33} = \alpha_{31} + \alpha_{23} \quad .$$

The effective strain rate becomes

$$\begin{aligned} \frac{\dot{\varepsilon}}{\varepsilon}^2 = \frac{1}{G^2} [& \alpha_{12}(\alpha_{23}\dot{\varepsilon}_{11} - \alpha_{31}\dot{\varepsilon}_{22})^2 + \alpha_{23}(\alpha_{31}\dot{\varepsilon}_{22} - \alpha_{12}\dot{\varepsilon}_{33})^2 \\ & + \alpha_{31}(\alpha_{12}\dot{\varepsilon}_{33} - \alpha_{23}\dot{\varepsilon}_{11})^2] \end{aligned} \quad (8)$$

with

$$G = \alpha_{12}\alpha_{23} + \alpha_{23}\alpha_{31} + \alpha_{31}\alpha_{12} \quad . \quad (9)$$

If we take $\alpha_{11} = 1$ for uniaxial testing in the with-grain direction, then

$$\frac{\dot{\varepsilon}}{\varepsilon} = \frac{c}{E_{11}} \bar{\sigma} = k\bar{\sigma} \quad , \quad (10)$$

$\dot{\varepsilon} = \dot{\varepsilon}_{11}$ and $\bar{\sigma} = \sigma_{11}$ for uniaxial testing, and

$$\dot{\lambda} = \frac{\dot{\varepsilon}}{\sigma} = \frac{c}{E_{11}} = k$$

where

E_{11} = Young's modulus in with-grain direction,

k = creep coefficient in with-grain direction.

For TSX graphite with rotational symmetry about the Z axis

$$\dot{\epsilon}_z = \dot{\epsilon}_{11} \quad , \quad \dot{\epsilon}_x = \dot{\epsilon}_{22} \quad , \quad \dot{\epsilon}_y = \dot{\epsilon}_{33} \quad ,$$

where $\dot{\epsilon}_x$ and $\dot{\epsilon}_y$ are two orthogonal axes normal to the Z axis, and

$$\alpha_{11} = 1, \alpha_{22} = \alpha_{33}, \alpha_{12} = \alpha_{31} = \frac{1}{2} \quad .$$

Because the experimental results from uniaxial testing show that the creep coefficient is related to Young's modulus as given in Eq. (10), it follows that

$$\alpha_{22} = \alpha_{33} = \frac{E_z}{E_x} = \frac{E_z}{E_y} \quad . \quad (11)$$

Therefore, in summary for TSX graphite,

$$\alpha_{11} = 1 \quad , \quad \alpha_{22} = \frac{13.5}{4.5} = 3.0 \quad , \quad \alpha_{12} = 0.5 \quad , \quad \alpha_{23} = 2.5 \quad , \quad (12)$$

and these yield the results

$$\frac{1}{\sigma^2} = 0.5(\sigma_z - \sigma_y)^2 + 2.5(\sigma_y - \sigma_z)^2 + 0.5(\sigma_x - \sigma_z)^2 \quad (13)$$

$$\begin{aligned} \frac{1}{\dot{\epsilon}^2} = \frac{1}{G^2} [& 0.5(2.5 \dot{\epsilon}_z - 0.5 \dot{\epsilon}_y)^2 + 2.5(0.5 \dot{\epsilon}_y - 0.5 \dot{\epsilon}_z)^2 \\ & + 0.5(0.5 \dot{\epsilon}_x - 2.5 \dot{\epsilon}_z)^2] \end{aligned} \quad (14)$$

with

$$G = 2.75$$

and

$$\dot{\epsilon}_z = k[\sigma_z - 0.5(\sigma_x + \sigma_y)] \quad (15)$$

$$\dot{\epsilon}_y = k[3.0 \sigma_y - 2.5 \sigma_x - 0.5 \sigma_z]$$

$$\dot{\epsilon}_x = k[3.0 \sigma_x - 2.5 \sigma_y - 0.5 \sigma_z] \quad .$$

Appendix B shows justification of Eqs. (12) through (15) for grade H327. Notice in Eq. (15) that the volume is not expected to be changed by creep. This is in agreement with the results at ORNL but is in conflict with results given by Price in his review. This is a result of the lack of recognition that Poisson's ratios are $d\lambda_1/d\lambda_2$ and not $\Delta\lambda_1/\Delta\lambda_2$. With the exception of ORNL's data, all of the data on transverse to longitudinal strain ratios were calculated including the primary creep. Because primary creep does cause a significant volume change, the ratio of the total strains can never show that the volume is constant.

As just mentioned, primary creep does produce a volume change. Primary creep has also been found to be anelastic in that full recovery is observed when the stress is removed. The time or fluence required for primary creep to fully saturate or recover is very short in contrast to the rate of loading under essentially all normal operating conditions except for rapid transients that cause thermal stresses. This permits the primary creep to be effectively included with the true elastic response as a single pseudo-elastic term. Because primary creep in the temperature range 400 to 600°C is essentially equal to the initial elastic strain, we have the following equations for elastic response of TSX:

$$\dot{\epsilon}_z = \left(\frac{\dot{\sigma}_z}{E_z} \right)_{\text{elastic}} + \left(\frac{\dot{\sigma}_z}{E_z} \right)_{\text{primary}} = \frac{2\dot{\sigma}_z}{E_z} \quad (16)$$

$$\dot{\epsilon}_x = \frac{2\dot{\sigma}_x}{E_x}, \quad \dot{\epsilon}_y = \frac{2\dot{\sigma}_y}{E_y}.$$

There is no Poisson's strain for primary creep, and it is virtually unmeasurable (<0.02) for simple elastic loading. This is not unusual for graphites made with highly acicular filler cokes, where even very fine-grained graphites have only a maximum of 0.05 for Poisson's ratio. This means that the major elastic response in TSX graphite is the opening or closing of the existing flaw structure, not a transverse displacement.

USEFUL LIFE AND APPROXIMATE STRESS CALCULATIONS

Estimates of useful life based on the fluence required to densify and then expand back to the original density are given in Fig. 23 for graphite grades TSX, H451, ATR-2E¹⁹ (a German second-generation graphite), and GraphNOL N3M¹³ (a third-generation graphite developed at ORNL). The increased life expectancy of the more advanced isotropic graphites is obvious. The results from Petten on grade ATR-2E to 300°C certainly give credibility to the exclusion of the lower temperature results reported by Helm. Estimates of the life expectancy should take into consideration the actual temperature and flux across the block. Therefore, credit can be taken for the lower temperatures in the higher-flux tube blocks. Shown in Table 1 are the results of estimates using an annual fluence to obtain a volume average of 2.4×10^{26} neutrons/m² ($E > 50$ keV) in the tube blocks by the year 2010.

Table 1. Estimated useful life of graphite components of the N-Reactor

Component		Temperature (°C)	Year 2010 fluence (neutrons/m ²) $E > 50$ keV	Life ratio ^a
Tube block	Inside diam	454	4.00×10^{26}	1.0
	Corners	500	2.56×10^{26}	0.73
Uncooled filler block	Tube face	504	2.84×10^{26}	0.81
	Center	545	2.44×10^{26}	0.79
Cooled filler block	Tube face	385	2.84×10^{26}	0.68
	Inside diam	275	2.44×10^{26}	0.55

^aRatio of 2010 fluence to zero volume fluence from Fig. 19. Determined by using peak fluence of 4×10^{26} neutrons/m² ($E > 50$ keV).

These estimates of useful life show that the inner surface of the tube block will begin to degrade sooner than other areas. There is some uncertainty in the cooled filler block operating at the very low temperature of 275°C. While increased life is expected with decreasing temperature to at least 400°C, there is a temperature where the growth rates

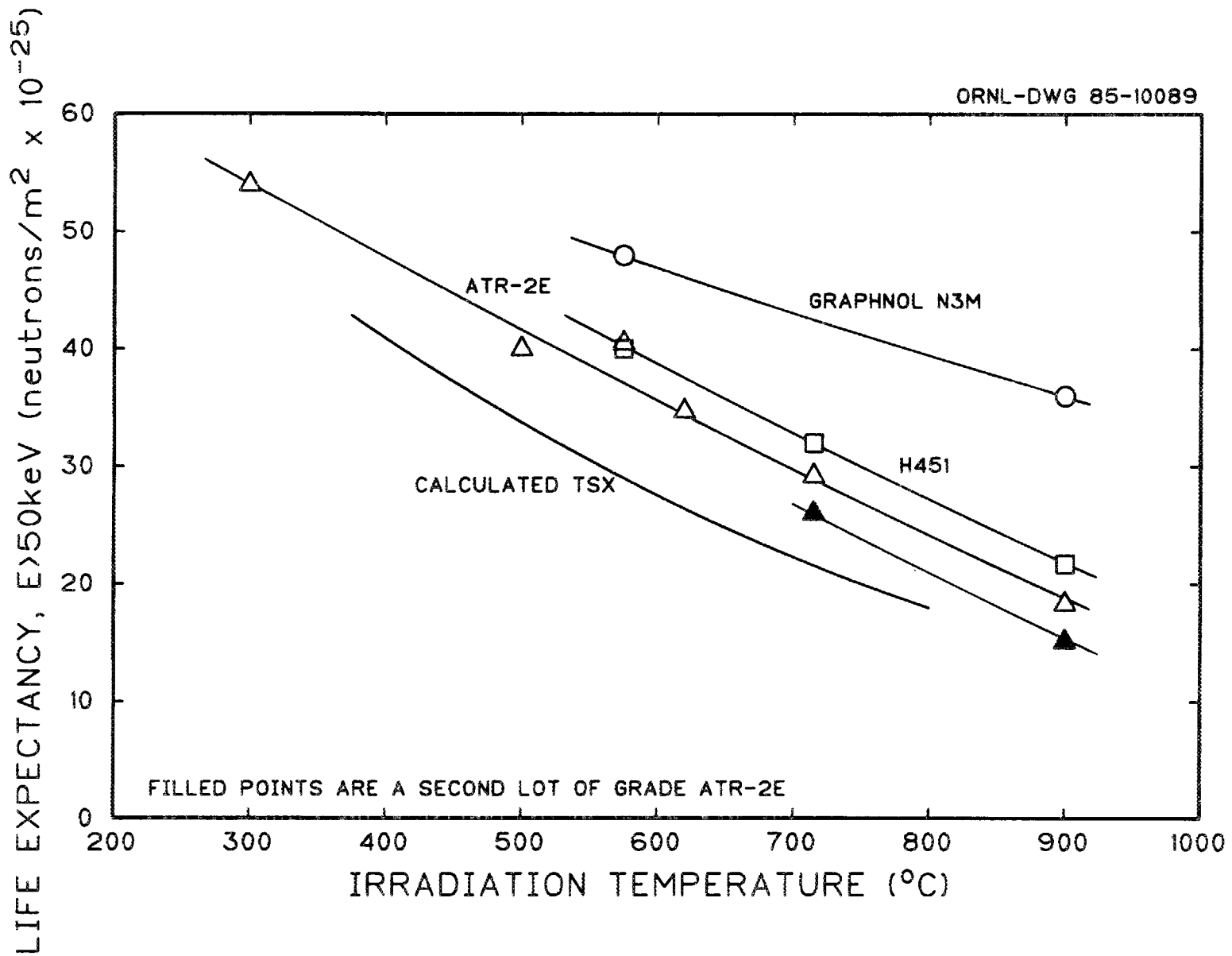


Fig. 23. Estimated useful life of various graphites.

will begin to increase. Thus, as the temperature is reduced below 400°C, the useful life will reach a maximum and then decrease. The Petten results tend to indicate that the temperature for maximum life is below 300°C for Grade ATR-2E, but it is undetermined for TSX graphite. The flux in the cooled filler block is reduced to about 60% of the peak flux, so it is doubtful that these blocks will lose their integrity before the tube blocks. Even if the inside diameter of the tube blocks loses its integrity, a structural analysis will almost certainly show that the block will not fail because of the support from the remainder of the block.

It is not within the scope of this report to perform a complete stress analysis of the core structure blocks. However, an approximate estimation of the stresses due to the filler block-tube block interaction may be in order to illustrate the magnitude of the generated stresses. The solution will not average the growth in the filler and tube blocks but will use volume average of temperatures and flux. In reality, the differential growth across the wall of the tube blocks and across the filler blocks will cause stresses that must be averaged with the block interaction stresses. The magnitude of the maximum axial stress in the tube block with a flux drop of about 1.5 could be as high as 6.9 MPa on the inside diameter of the block. In the keyed structure, the growth rate difference between blocks will be equal to zero. The following equations are used for the dimensional changes for the filler-block keys:

$$\dot{\epsilon}_{zf} = \frac{\dot{\sigma}_{zf}}{E_z} + \frac{\dot{\sigma}_{zf}}{E_z} + k\phi_f(\sigma_{zf} - 0.5 \sigma_{xf}) + \dot{g}_{zf}\phi_f + \frac{d}{dt} \alpha_z \Delta T_f \quad (17a)$$

(elastic creep)
(primary creep)
(secondary creep)
(irradiation growth)
(thermal strain)

$$\dot{\epsilon}_{xt} = \frac{\dot{\sigma}_{xt}}{E_x} + \frac{\dot{\sigma}_{xt}}{E_x} + k\phi_t (0.3 \sigma_{xt} - 0.5 \sigma_{zt}) + \dot{g}_{xt}\phi_t + \frac{d}{dt} \alpha_x \Delta T_t \quad (17b)$$

with the coupling condition

$$\epsilon_{zf} - \epsilon_{xt} + \frac{\Delta}{6} = 0 \quad ,$$

where

$\dot{\epsilon}_{zf}$ = filler-block strain rate in the axial direction,

$\dot{\epsilon}_{xt}$ = tube-block strain rate in the transverse direction,

Δ = tolerance between the 6-in.-wide blocks initially,

k = uniaxial creep coefficient in the with-grain direction (see Eq. 10).

For the tube-block keys,

$$\dot{\epsilon}_{zt} = \frac{\dot{\sigma}_{zt}}{E_z} + \frac{\dot{\sigma}_{zt}}{E_z} = k\phi_t(\sigma_{zt} - 0.5 \sigma_{xt}) + \dot{g}_{zt}\phi_t + \frac{d}{dt} \alpha_z \Delta \Gamma_t \quad (18a)$$

$$\dot{\epsilon}_{xf} = \frac{\dot{\sigma}_{xf}}{E_x} + \frac{\dot{\sigma}_{xf}}{E_x} + k\phi_f(3.0 \sigma_{xf} - 0.5 \sigma_{zf}) + \dot{g}_{xf}\phi_f + \frac{d}{dt} \alpha_x \Delta \Gamma_f \quad (18b)$$

again coupled by

$$\epsilon_{zf} - \epsilon_{xf} + \frac{\Delta}{6} = 0 \quad ,$$

where

$\dot{\epsilon}_{zt}$ = tube-block strain rate in the axial direction,

$\dot{\epsilon}_{xt}$ = tube-block strain rate in the transverse direction.

From the geometry of the keys,

$$\sigma_{zf} = \frac{1.25}{1.75} \sigma_{xt} \quad , \quad \sigma_{xf} = -8.07 \sigma_{zt} \quad . \quad (19)$$

Substituting, combining, and using $\phi_f = 0.81 \phi_t$, we obtain the results

$$\begin{aligned} & \left(\frac{2}{E_z} + \frac{2.8}{E_x} \right) \sigma_{zf} + k\phi_t (5.01 \sigma_{zf} - 0.467 \sigma_{zf}) \\ & = (\dot{g}_{xt} - 0.81 \dot{g}_{zf}) \phi_t + \frac{d}{dt} (\alpha_x \Delta \Gamma_t - \alpha_z \Delta \Gamma_f) \quad , \end{aligned} \quad (20)$$

$$\begin{aligned} & \left(\frac{0.248}{E_z} + \frac{1.2}{E_x} \right) \sigma_{xf} + k\phi_t (2.55 \sigma_{xf} - 0.405 \sigma_{zf}) \quad (21) \\ & = (\dot{g}_{zt} - 0.81 \dot{g}_{xf}) \phi_t + \frac{d}{dt} (\alpha_z \Delta T_t - \alpha_x \Delta T_f) . \end{aligned}$$

The result is two differential equations with two unknowns. The differential growth is given by Eq. (2), which is a cubic equation in the fluence γ . The actual differential growth differences are shown in Fig. 24 for both the tube block-hot filler block and the tube block-cooled filler block interactions. At present, the integration of Eqs. (20) and (21) with the growth rates either a linear or parabolic function of fluence does not appear to be straightforward, and iterative methods will require additional effort. If the growth-rate differences are taken as constants for a given increment of fluence and the stress rates were essentially constant, a quick approximation of the stresses can be made.

For the volume averaged tube-block fluence from 1 to 2×10^{26} neutrons/m², and letting the differential growth rate between the tube block and either the filler block or the cooled filler block be approximated by

$$\begin{aligned} \dot{g}_{xt} - 0.81 \dot{g}_{zf} &= 3.0 \times 10^{-3} \\ 0.81 \dot{g}_{xf} - \dot{g}_{zt} &= 2.8 \times 10^{-3} , \end{aligned}$$

and substituting these values into Eqs. (20) and (21) yields

$$\begin{aligned} 4.13 \times 10^{-10} \sigma_{zf} - 3.03 \times 10^{-11} \sigma_{xf} &= 3.0 \times 10^{-3} \\ -9.08 \times 10^{-11} \sigma_{zf} + 2.10 \times 10^{-10} \sigma_{xf} &= 2.8 \times 10^{-3} , \end{aligned}$$

with the fluence in units of 10^{25} neutrons/m² ($E > 50$ keV). These equations can be readily solved to give

$$\begin{aligned} \sigma_{xf} &= -10.6 \text{ MPa } (-1530 \text{ psi}) \\ \sigma_{zf} &= 6.9 \text{ MPa } (910 \text{ psi}) . \end{aligned}$$

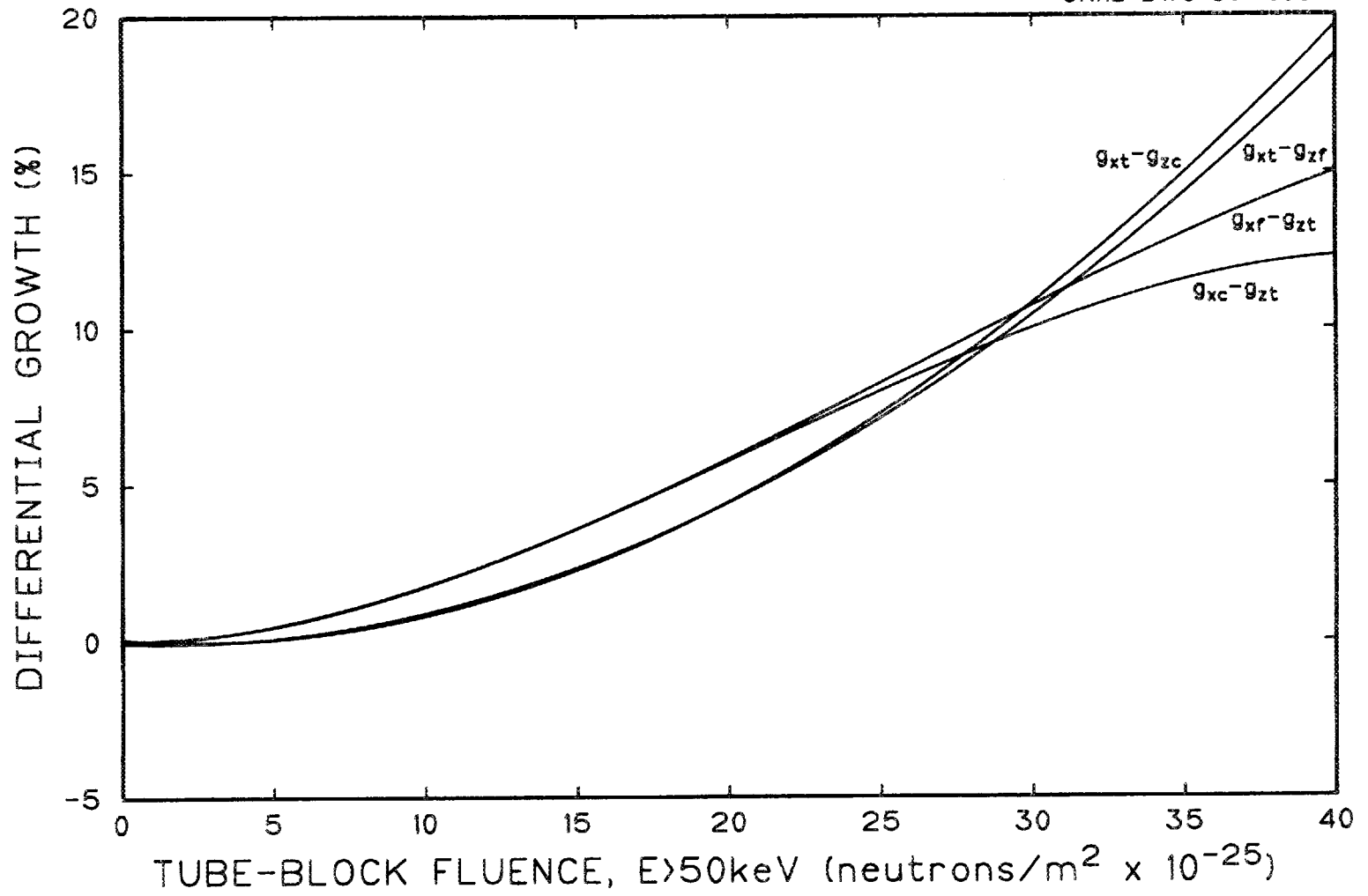


Fig. 24. Differential growth between tube blocks and filler blocks.

It requires about 40 kN (9000 lb) force²¹ to break the filler-block keys; therefore, it would be expected that the keys would begin to fail sometime after 1×10^{26} neutrons/m² (in 1977). The stress intensity will continue to increase until all of the keys fail, as can be shown by the calculations from 2 to 4×10^{26} neutrons/m² where $\dot{g}_{xt} - 0.81 \dot{g}_{zf}$ increases to 6×10^{-3} .

From 2 to 4×10^{26} neutrons/m²:

$$\sigma_{xf} = -7.34 \text{ MPa } (-1060 \text{ psi})$$

$$\sigma_{zf} = 14.1 \text{ MPa } (2050 \text{ psi})$$

$$\sigma_{xt} = -19.7 \text{ MPa } (-2860 \text{ psi})$$

$$\sigma_{zt} = 0.91 \text{ MPa } (130 \text{ psi}).$$

The stress in the filler block now produces a force of 80 kN (18,000 lb), more than twice that required to break the keys. All of the constrained filler-block keys will fail eventually. After the filler-block key fails, the stress state is now only controlled by the tube-block key interaction.

After the filler-block key is broken:

$$\sigma_{zf} = 0, \quad \sigma_{xt} = 0.$$

Thus:

$$\dot{\epsilon}_{xf} = \frac{2\dot{\sigma}_{xf}}{E_x} + k\phi_f \cdot 3.0 \sigma_{xf} + \dot{g}_{xf}\phi_f + \frac{d}{dt} \alpha_x \Delta T_f$$

$$\dot{\epsilon}_{zt} = \frac{2\dot{\sigma}_{zt}}{E_z} + k\phi_t + \dot{g}_{zt}\phi_t + \frac{d}{dt} \alpha_z \Delta T_t$$

or, on substituting for σ_{zt} and ϕ_f and equating

$$\begin{aligned} & \left(\frac{2}{E_x} + \frac{0.248}{E_z} \right) \dot{\sigma}_{xf} + k\phi_t (2.43 + 0.124) \sigma_{xf} \\ & = (\dot{g}_{zt} - 0.81 \dot{g}_{xf}) \phi_t + \frac{d}{dt} (\alpha_z \Delta T_t - \alpha_x \Delta T_f). \end{aligned}$$

This equation can be integrated if the stress states in the filler-block keys are known. Again, for simplicity, the growth rate difference ($g_{zt} - 0.81 g_{zt}$) is approximated by a constant of -2.8×10^{-3} , giving

$$\sigma_{xf} = -14.0 \text{ MPa } (-2030 \text{ psi})$$

$$\sigma_{zt} = 1.73 \text{ MPa } (250 \text{ psi}) .$$

The rather trivial increase in the axial stress by the broken filler-block key does not appear to be great enough to cause the tube-block keys to fail. Although the tube-block keys will not fail, there will be a strong tendency for the filler blocks to jump out of the 6.4-mm-deep (1/4 in.) slots in the tube blocks. This will be countered by the weight of the stack holding the blocks in place. Thus, as has been observed, some of the filler blocks have jumped out of the slots at the top of the stack. This dislocation may work its way down the stack as the stresses and the resulting forces increase with fluence.

The stack height should reflect some dimensional increase due to the plastic-creep deformation in the filler block-tube block interaction.

$$\dot{\epsilon}_{yt} = k\phi_t(-2.5 \sigma_{xt} - 0.5 \sigma_{zt}) + \dot{g}_{yt}\phi_t + \frac{d}{dt} \alpha_x \Delta T_t$$

$$\dot{\epsilon}_{yf} = k\phi_f(-2.5 \sigma_{xf} - 0.5 \sigma_{zf}) + \dot{g}_{yf}\phi_f + \frac{d}{dt} \alpha_x \Delta T_f .$$

Before fracture (up to 2×10^{26} neutrons/m²), assume the stresses on the average are only about one-half that calculated at the end point.

Then

$$\dot{\epsilon}_{yt} - \dot{g}_{yt}\phi_t = k (11.5 - 0.30) \cdot 0.45 = 0.0004/10^{21}$$

$$\dot{\epsilon}_{yf} - \dot{g}_{yf}\phi_f = k (13.8 - 1.60) \cdot 0.14 = 0.00014/10^{21}$$

or a total of 1.0% in 2×10^{26} neutrons/m². This is not large but could add as much as an inch to the overall stack height. The increase

after the key is broken results only from the stresses in the filler block. Again, using one-half of the calculated stress intensities, we obtain

$$\dot{\epsilon}_{yt} - \dot{g}_{yt}\phi_t = k(-0.40) \cdot 0.45 = 0.0001/10^{21}$$

$$\dot{\epsilon}_{yf} - \dot{g}_{yf}\phi_t = k(18.2) \cdot 0.14 = 0.0002/10^{21}.$$

In this case, there is only about 0.2% increase in 2×10^{26} neutrons/m², which will not add much to the stack height. The breaking of the filler keys will reduce the stack-height growth from creep deformation.

SUMMARY

The effect of irradiation on the physical properties of graphite has been discussed. In general, there are two types of irradiation damage that affect these properties. The first is the production of vacancy clusters and the second is the structural changes that result from the anisotropic crystallite growth. Those properties affected by vacancy cluster density, such as conductivity and elastic moduli, change very rapidly and the change saturates as the defect density saturates. All the properties are affected by the structural changes within the graphite, particularly after the fluence required to obtain maximum density is obtained. As the volume increases, most of the properties are detrimentally affected. All available information indicates that the physical properties, such as strength, elastic moduli, conductivity, and CTE, are not seriously degraded up to the fluence required to increase the volume to the original density. The extent to which these properties can be permitted to degrade by volume expansion needs to be examined carefully.

The dimensional changes of TSX graphite as a function of temperature and fluence have been estimated. These estimates were based on some TSX data and, to a larger extent, on data for other similar graphites and the more advanced isotropic grades that have been irradiated to higher fluences. The effects of irradiation on properties such as elastic moduli, conductivity, and CTE were based on TSX data and extrapolated by using the estimates of dimensional changes.

The irradiation creep characteristics of TSX graphite were estimated on the basis of very similar grades. The estimation of the creep behavior after maximum density was based on results from Petten on a German isotropic grade graphite.

Very crude approximations of the stresses generated by the keyed structure have been made by using the creep characteristics. The constrained filler-block keys will certainly fracture before the year 2000. The estimate of the initiation of the key failure is in rough agreement with the observations. After the filler-block keys fail, the stresses from the tube-block key interaction increase. Those stresses, however, should not be high enough to cause the tube-block keys to fail. The overall increase in vertical growth due to creep is estimated to be about 25 to 38 mm (1-1.5 in.) overall.

These are only crude estimates, and a more accurate analysis should be done. The coefficients included in this report should allow an orderly analysis of the stresses in the stack. The analysis certainly should be done if the growth in the stack height is of concern.

ACKNOWLEDGMENTS

I would like to thank R. J. Lauf and J M Robbins for their thoughtful reviews of this report. I would also like to acknowledge the assistance of F. P. Jeffers in the preparation of the figures and of M. B. White in typing the manuscript. O. A. Nelson edited the report, and Mary Rhea and P. H. Wilson prepared the final manuscript.

REFERENCES

1. D. R. deHalas, *Nuclear Graphite*, ed. R. E. Nightingale, Academic Press, New York, 1962, p. 195.
2. W. N. Reynolds, "Radiation Damage in Graphite," *Chemistry and Physics of Carbon*, ed. P. L. Walker, Jr., Marcel Dekker, New York, 1966, p. 121.

3. J. H. W. Simmons, *Radiation Damage in Graphite*, Pergamon Press, New York, 1965.
4. B. T. Kelly et al., "Dimensional Changes in Polycrystalline Graphites Under Fast-Neutron Irradiation," *Philos. Trans. Roy. Soc. London*, Ser. A, No. 1109, 260, 51-71 (1966).
5. P. A. Throver, *Chemistry and Physics of Carbon*, ed. P. L. Walker, Marcel Dekker, New York, 1969.
6. G. B. Engle and W. P. Eatherly, "Irradiation Behavior of Graphite at High Temperature," *High Temp.-High Pressures* 4, 119-58 (1972).
7. J. C. Bokros and R. J. Price, "Dimensional Changes Induced in Pyrolytic Carbon by High-Temperature Fast-Neutron Irradiation," *Carbon* 5, 301 (1967).
8. G. E. Bacon, "A Method for Determining the Degree of Orientation of Graphite," *J. Appl. Chem.* 6, 477-81 (1956).
9. R. J. Price and J. C. Bokros, "Relationships Between Preferred Orientation, Thermal Expansion, and Radiation Length Changes in Graphite," *J. Appl. Phys.* 36, 1897-1906 (1965).
10. B. W. Ashton, J. E. Brocklehurst, and B. T. Kelly, "The Effect of Fast Neutron Irradiation on the Pore Structure of Reactor Moderator Graphites," p. 310 in *11th Biennial Conference on Carbon Extended Abstracts and Program, June 4-8, 1973, Gatlinburg, Tennessee*, American Carbon Society, 1973.
11. C. R. Kennedy, W. P. Eatherly, and D. Mindermann, "A Comparison of the Characteristics of Graphite Irradiated at 600 to 900°C," p. 544 in *16th Biennial Conference on Carbon Extended Abstracts and Program, July 18-22, 1983, University of California, San Diego, Calif.*, American Carbon Society, 1983.
12. C. R. Kennedy, "The Effect of Irradiation on the Fracture Toughness of Graphite," to be published in *17th Biennial Conference on Carbon Extended Abstracts and Program, June 16-21, 1985, University of Kentucky, Lexington, Kentucky*, American Carbon Society, 1985.
13. C. R. Kennedy, "Evaluation at Fracture Strength by Sonic Testing," p. 536 in *15th Biennial Conference on Carbon Extended Abstracts and Program, June 22-23, 1981, Philadelphia, Pennsylvania*, American Carbon Society, 1981.

14. J. W. Helm, *Irradiation of Graphite at Temperatures of 300-1200°C*, USAEC Report BNWL-1056A, Battelle Northwest Laboratory, Richland, Wash., 1969.
15. R. W. Henson, A. J. Perks, and J. A. E. Simmons, "Lattice Parameters and Dimensional Changes in Graphite Irradiated Between 300 and 1350°C," *Carbon* 6, 789 (1968).
16. M. F. O'Connor et al., "Suitability Tests for HTR Reflector," Carbon Conference, Baden Baden, Federal Republic of Germany, 1980.
17. R. J. Price, "A Review of the Thermal Conductivity of Graphite under HTGR Conditions," GA-A12615, Gulf General Atomic, San Diego, Calif., 1973.
18. R. J. Price, "Irradiation Induced Creep in Graphite, A Review," GA-A16402, Gulf General Atomic, San Diego, Calif., 1981.
19. M. A. Cundy and G. Kleist, "Irradiation Creep to Very High Neutron Fluences," p. 406 in *Transactions Carbone 84*, Bordeaux, France, 1984.
20. L. W. Hu, "Studies on Plastic Flow of Anisotropic Materials," *J. Appl. Mech.* 21, 444-50 (1950).
21. W. C. Morgan, *N-Reactor Stack Integrity*, BNWL-CC-455, Battelle Northwest Laboratory, Richland, Wash., 1966.

APPENDIX A. THERMAL CONDUCTIVITY DATA

This appendix is an excerpt (pp. 44-48) from report Gulf-GA-A-12615 (GA-LTR-3), *Review of the Thermal Conductivity of Nuclear Graphite Under HTGR Conditions*, by R. J. Price, Sept. 7, 1973, Gulf General Atomic Company (now GA Technologies, Inc.), P.O. Box 81608, San Diego, CA 92138.

5. CONSOLIDATION OF DATA: DEPENDENCE ON FLUENCE, IRRADIATION TEMPERATURE, AND MATERIAL

5.1 Approach to Saturation

The experimental data discussed earlier in this report show that irradiation reduces the thermal conductivity of a given grade of graphite, with the rate of decline falling off and approaching saturation as the fluence increases. This behavior pattern holds up to the onset of breakaway expansion and may be represented by an expression of the type:

$$K = K_{\text{sat}} + \left(K_0 - K_{\text{sat}} \right) \exp \left(- \frac{\phi t}{\tau} \right) \quad (4)$$

where K is the conductivity after a fluence (ϕt), K_0 is the 'unirradiated thermal conductivity, K_{sat} the conductivity after irradiation to saturation, and τ is the "time constant" (actually a fluence) for saturation. The number of measurements with sufficient low-fluence data points to estimate τ is limited, but time constants estimated from several sets of data are plotted in fig. 22 as a function of irradiation temperature. Fluences are expressed in terms of neutrons with energies greater than 0.18 MeV. No systematic difference between different types of graphite is visible. A least-squares linear regression analysis for the data in fig. 22 gives the following empirical equation for the time constant, τ , as a function of irradiation temperature, $T(^{\circ}\text{C})$:

$$\tau = \left[(1.589 \pm 0.677) \times 10^{-3} T - (0.641 \pm 0.581) \right] \times 10^{21} \text{ n/cm}^2 \quad (E > 0.18 \text{ MeV})$$

where the error limits represent 90% confidence limits on the parameters.

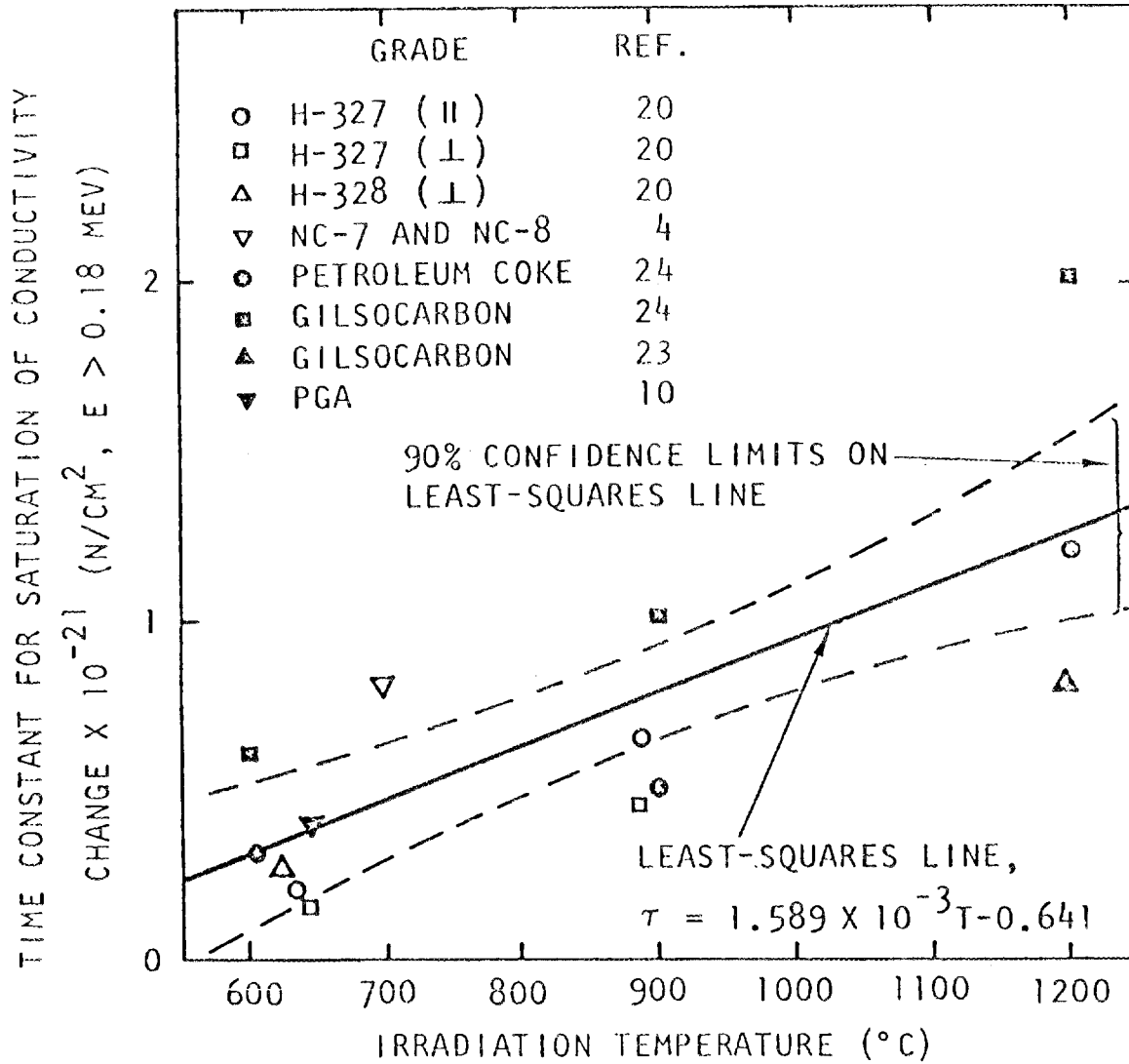


Fig. 22. Composite plot of the time constant for the saturation of the thermal conductivity change as a function of irradiation temperature

5.2 Conductivity after Irradiation to Saturation

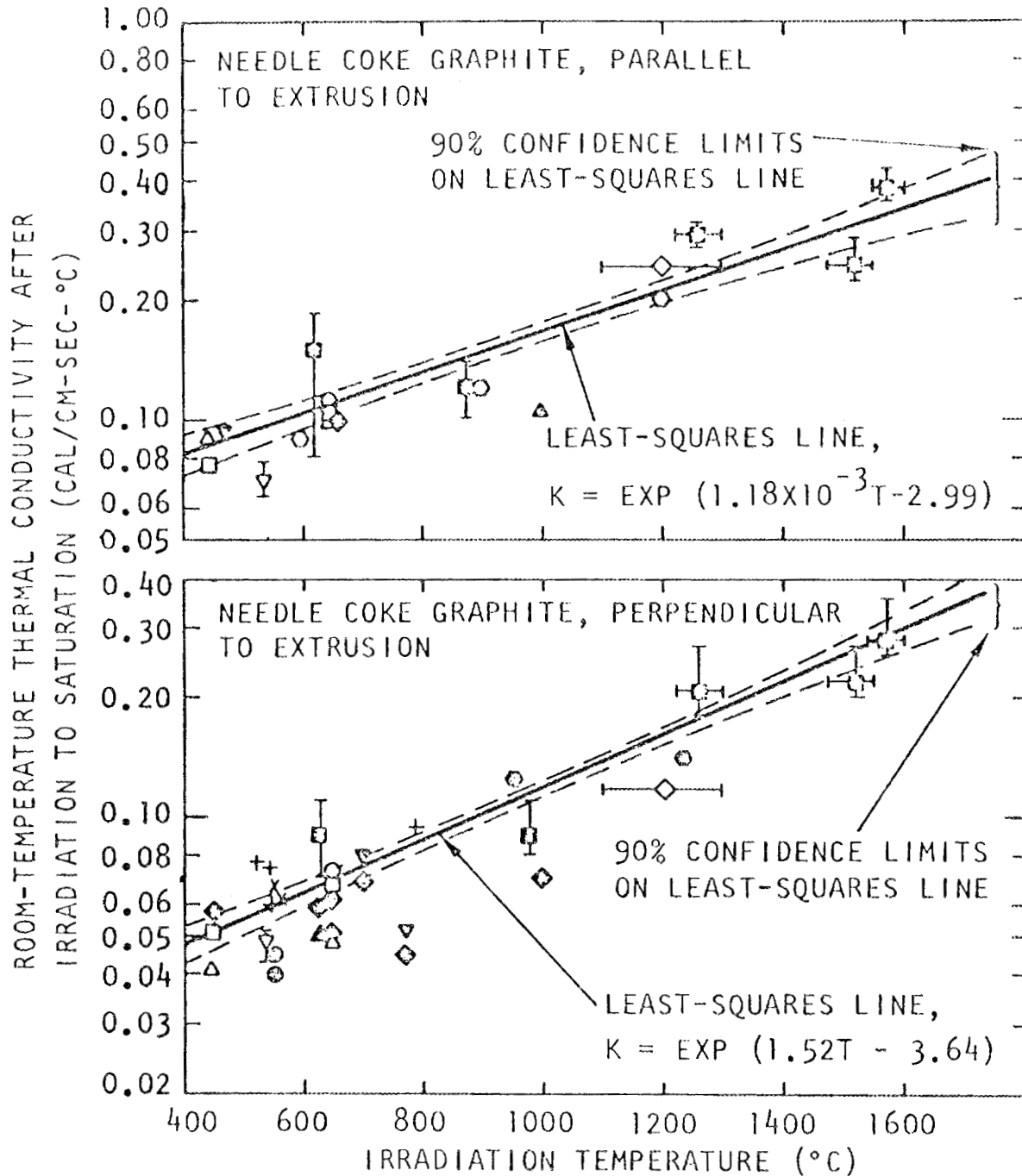
After irradiation to a fluence high enough for saturation to occur but too low for breakaway expansion to start, the thermal conductivity is dependent only on the irradiation temperature and the grade and orientation of the graphite. The temperature dependence can best be determined empirically by lumping together all available data on a given type of graphite irradiated to a fluence high enough for saturation to have occurred. This procedure was followed in constructing figs. 23 and 24, where room-temperature conductivities taken from the literature are plotted against irradiation temperature for needle-coke graphites (parallel and perpendicular) and isotropic (Gilsocarbon-based) graphites. Some lower-fluence data were also included by extrapolating the measurements to saturation, using eq. 4. High-fluence measurements affected by sample expansion, and the data of doubtful reliability from capsule G-12, were excluded from the plot. It may be seen that the saturated conductivity rises exponentially with increasing irradiation temperature over the temperature range 400°C to 1600°C. Least-squares regression analysis of the data in figs. 23 and 24 yields the following empirical expressions for the conductivity after irradiation to saturation, K_{sat} , in terms of the irradiation temperature, $T(^{\circ}\text{C})$:

Needle coke graphite, parallel to extrusion:
$$K_{sat} = \exp \left[(1.18 \pm 0.17) \times 10^{-3}T - (2.99 \pm 0.18) \right]$$
 cal/cm-sec-°C

Needle coke graphite, perpendicular to extrusion:
$$K_{sat} = \exp \left[(1.52 \pm 0.12) \times 10^{-3}T - (3.64 \pm 0.12) \right]$$
 cal/cm-sec-°C

Gilsocarbon graphite, any direction:
$$K_{sat} = \exp \left[(1.20 \pm 0.22) \times 10^{-3}T - (3.31 \pm 0.26) \right]$$
 cal/cm-sec-°C

The \pm figures are 90% confidence limits calculated from the curve-fitting statistics.



GRADE	REF.	GRADE	REF.	GRADE	REF.
○ PGA	2	○ 59/2	12	◇ TSX	4
□ PGA	8	● H-327	18	● CHN	5
△ PGA	10	■ H-327	20	+ TS-688	18
▽ PGA	11	△ NC-8	4	x 9567	18
◇ PGA	13	▽ CSF	4		

Fig. 23. Composite plot of the room-temperature thermal conductivity of needle-coke graphites irradiated to saturation as a function of irradiation temperature

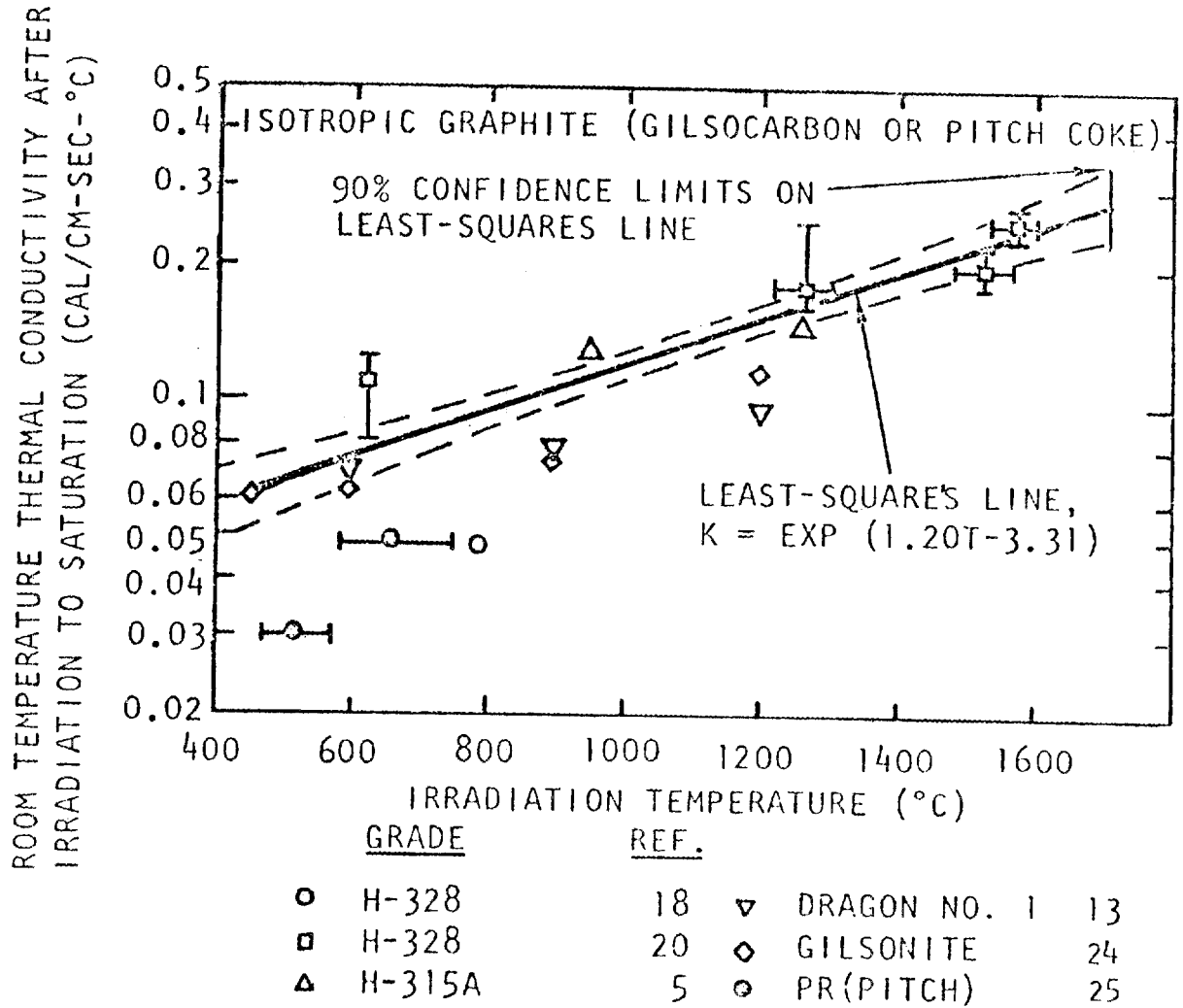


Fig. 24. Composite plot of the room temperature thermal conductivity of Gilsocarbon and pitch coke graphites irradiated to saturation as a function of irradiation temperature

APPENDIX B. CONFIRMATION OF EQUATION 15

Graphite creep experiments OC1, OC3, and OC5 run in the Oak Ridge Research Reactor had both axial and radial specimens of grade H327 loaded in compression at 900°C. Graphite grade H327, like grade TSX, is fairly anisotropic and has the following elastic constants:

$$\begin{aligned} E_z &= 11.47 \text{ GPa} & S_{12}/S_{11} &= 0.08 \\ E_r &= 5.79 \text{ GPa} & S_{13}/S_{11} &= 0.01 \\ G_{44} &= 3.65 \text{ GPa} & S_{13}/S_{33} &= 0.02 \\ G_{66} &= 2.69 \text{ GPa} \end{aligned}$$

These values yield

$$\begin{aligned} \alpha_{11} &= 1, \quad \alpha_{22} = \alpha_{33} = \frac{E_z}{E_r} = 2.0, \\ \alpha_{12} &= \alpha_{31} = 0.5, \quad \text{and} \quad \alpha_{23} = 1.5 \\ \bar{\sigma}^2 &= 0.5(\sigma_z - \sigma_y)^2 + 1.5(\sigma_y - \sigma_z)^2 + 0.5(\sigma_x - \sigma_z)^2 \\ \frac{\dot{\epsilon}}{\epsilon^2} &= \frac{1}{G^2} [0.5(1.5\dot{\epsilon}_z - 0.5\dot{\epsilon}_y)^2 + 1.5(0.5\dot{\epsilon}_y - 0.5\dot{\epsilon}_z)^2 \\ &\quad + 0.5(0.5\dot{\epsilon}_x - 1.5\dot{\epsilon}_z)^2] \end{aligned} \quad (\text{B.1})$$

$$G = 1.75,$$

and

$$\begin{aligned} \dot{\epsilon}_z &= K[\sigma_z - 0.5(\sigma_x + \sigma_y)] \\ \dot{\epsilon}_y &= K(2.0\sigma_y - 1.5\sigma_x - 0.5\sigma_z) \\ \dot{\epsilon}_x &= K(2.0\sigma_x - 1.5\sigma_y - 0.5\sigma_z). \end{aligned} \quad (\text{B.2})$$

The diameters of axial and radial specimens compressively loaded to 13.8 MPa were measured. In the case of the radial specimen, careful attention was given to determine the maximum and minimum diameters. The diameter measurements can be used to confirm the above equations as well as to demonstrate that primary creep occurs only in the loaded direction. The results of the measurements are given in Figs. B.1 and B.2. The data clearly show that the primary creep does not have a Poisson's ratio and does produce a volume change in the graphite. The diameter strain rates in the axially stressed specimen are essentially the same

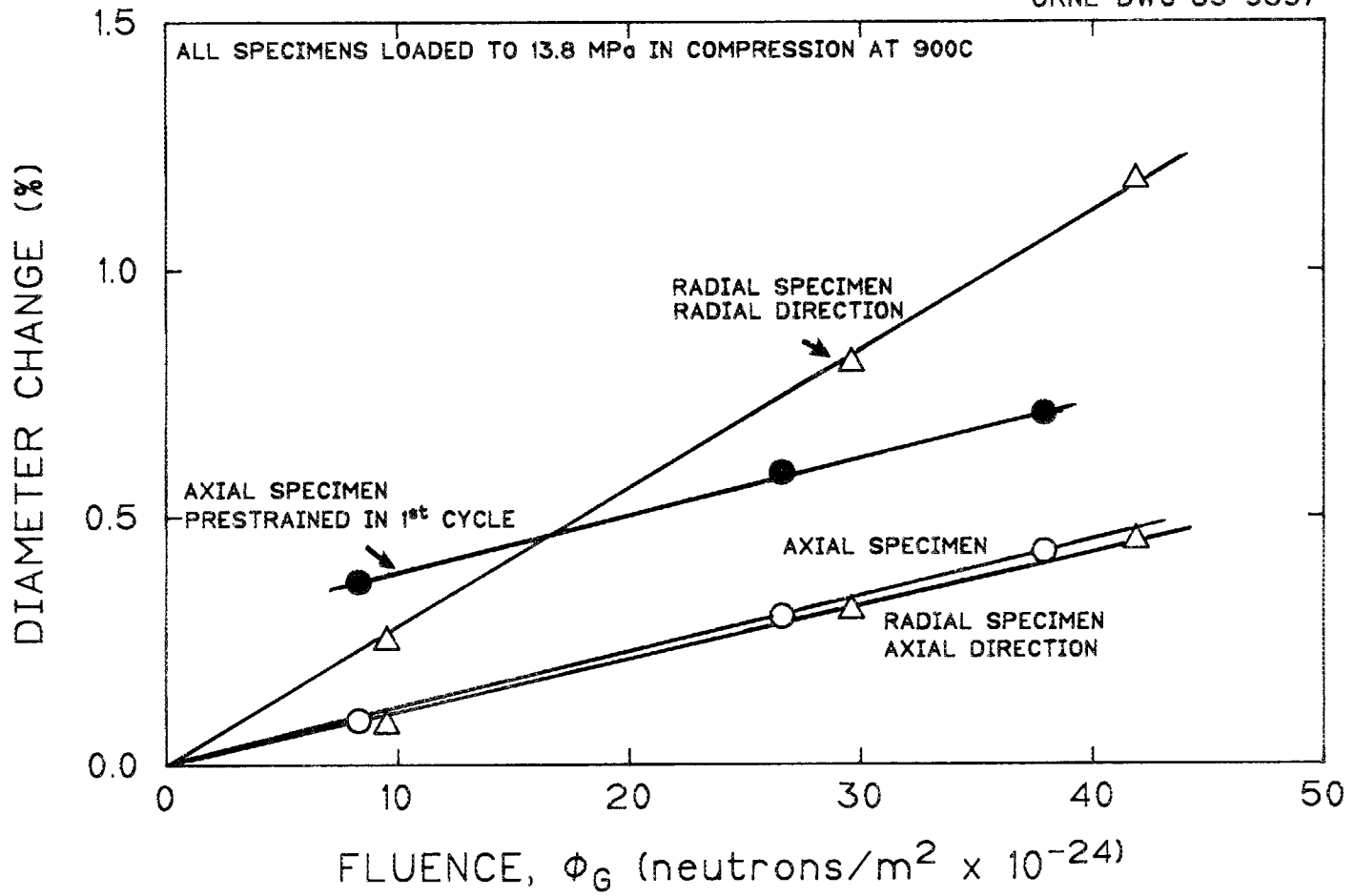


Fig. B.1. Diameter changes due to creep of graphite grade H327.

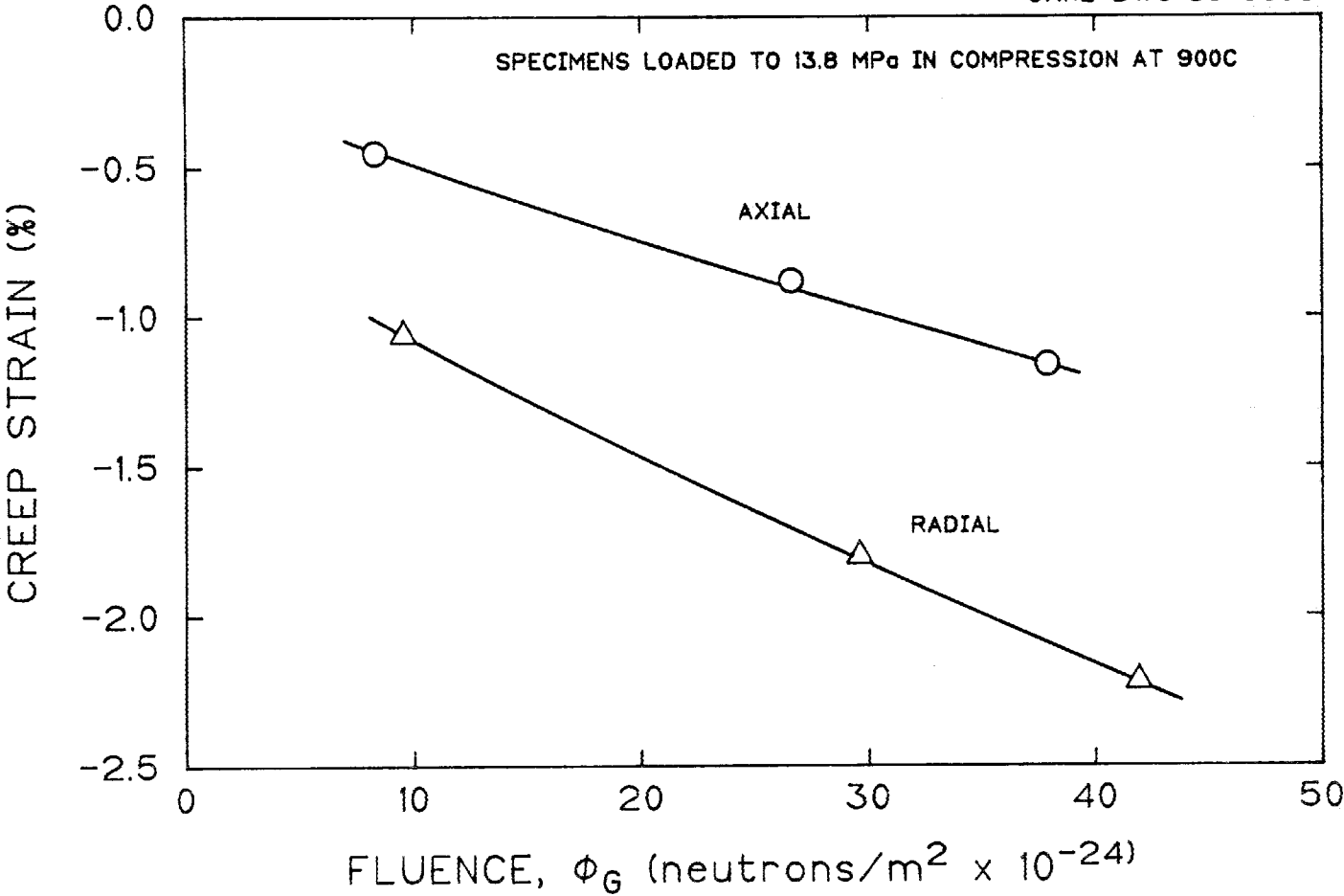


Fig. B.2. Creep of graphite grade H327 at 900°C in compression.

as the strain rate in the axial direction of a radially stressed specimen as expected from Eq. (B.2). The ratio of the minimum and maximum strain rates in the radially stressed specimen is 2.6, very close to a 3.0 expected from Eq. (B.2). The K value for H327 at 900°C is 1.75×10^{-35} from the axial specimen and 1.89×10^{-35} from the radial specimen, which is very close to the 1.72×10^{-35} calculated from Eq. (6) in the text. These overall results are very persuasive in confirming the validity of Eq. (15) in the text.

INTERNAL DISTRIBUTION

- 1-2. Central Research Library
- 3. Document Reference Section
- 4-5. Laboratory Records Department
- 6. Laboratory Records, ORNL RC
- 7. ORNL Patent Section
- 8. W. P. Eatherly
- 9-13. C. R. Kennedy
- 14-16. P. T. Thornton

EXTERNAL DISTRIBUTION

- 17. DOE, OAK RIDGE OPERATIONS OFFICE, P.O. Box E, Oak Ridge,
TN 37831
Assistant Manager for Energy Research and Development
- 18-44. DOE, TECHNICAL INFORMATION CENTER, P.O. Box 62, Oak Ridge,
TN 37831